Interaction and Multiscale Mechanics, Vol. 1, No. 1 (2007) 53-81
DOI: http://dx.doi.org/10.12989/imm.2007.1.1.053

A transport model for high-frequency vibrational power flows in coupled heterogeneous structures

Éric Savin†

Structural Dynamics and Coupled Systems Department, ONERA,
29, Avenue de la Division Leclerc, 92322 Châtillon Cedex, France

(Received July 31, 2007, Accepted November 11, 2007)

Abstract. The theory of microlocal analysis of hyperbolic partial differential equations shows that the energy density associated to their high-frequency solutions satisfies transport equations, or radiative transfer equations for randomly heterogeneous materials with correlation lengths comparable to the (small) wavelength. The main limitation to the existing developments is the consideration of boundary or interface conditions for the energy and power flow densities. This paper deals with the high-frequency transport regime in coupled heterogeneous structures. An analytical model for the derivation of high-frequency power flow reflection/transmission coefficients at a beam or a plate junction is proposed. These results may be used in subsequent computations to solve numerically the transport equations for coupled systems, including interface conditions. Applications of this research concern the prediction of the transient response of slender structures impacted by acoustic or mechanical shocks.

Keywords: vibration; high-frequency; transport; interface; coupling.

1. Introduction

Elastic structures exhibit typical transport and diffusive behaviors in their higher frequency range of vibration. Two approaches are currently used by engineers to predict and quantify such phenomena. Statistical energy analysis (SEA), see e.g., Lyon and DeJong (1995) is a global approach in the sense that it gives uniform estimates of the mean vibrational energy within substructures of a complex mechanical system. A major difficulty of the method, which is still very heuristic, is the estimation of the physical parameters of the formulation: loss factors, coupling loss factors, modal densities, and input powers. The vibrational conductivity analogy of structural acoustics, or power flow analysis (Nefske and Sung 1989), is a local model inasmuch as it intends to estimate the vibrational energy and power flow *densities*. However its developments are restricted to simple homogeneous structures (beams and more rarely plates) because it is based on some very restrictive hypotheses which are difficult to fulfil - or are simply wrong - for more complex structures (Bouthier and Bernhard 1992, Langley 1995, Lase *et al*. 1996).

The modern mathematical theory of microlocal analysis shows that the energy density associated to high-frequency elastic waves satisfy Liouville-type transport equations (Gérard *et al*. 1997, Guo and Wang 1999, Lions and Paul 1993, Papanicolaou and Ryzhik 1999). It generalizes both previous

† E-mail: Eric.Savin@onera.fr

methods and alleviates a great deal of their inconsistency. The analysis is based on the use of a Wigner transform and an explicit scaling of wave propagation patterns. The high-frequency, non-negative limit of the Wigner transform is the so-called Wigner measure, which is an angularly resolved energy density in time and phase space. This quantity also characterizes the power flows within the medium, and may be used to track the energy paths. The main shortcoming of the theory to date is the consideration of boundary and interface conditions for energetic observables consistent with the boundary/interface conditions imposed to the displacement and stress fields. Some preliminary results were given in Miller (2000) for the high-frequency solutions of a scalar wave equation accross a sharp interface between two heterogeneous media, or in Akian (2006), Burq and Lebeau (2001) for the Lamé system in a bounded smooth domain with Dirichlet boundary conditions. Their generalization to arbitrary boundary conditions is the subject of ongoing research. The energy density in bounded media may be characterized by the Wigner measures of the true solutions as done in Akian (2003, 2006), Gérard *et al*. (1997), Guo and Wang (1999), Lions and Paul (1993), Miller (2000), Papanicolaou and Ryzhik (1999), or the explicit Wigner measures of approximate solutions (which coincide with the Wigner measures of the true solutions) as initiated by Bougacha *et al*. (2007). Such approximate solutions are constructed as the superposition of Gaussian beams for arbitrary initial conditions, and they allow to account for the boundary conditions within convex domains. For non-convex domains, other classes of approximations need be introduced. In this paper we focus on the formal development of boundary and interface conditions for coupled heterogeneous beams or plates. Our derivation of power flow reflection/transmission coefficients for the junction is based on a wave analysis, where the wave components are obtained from the high-frequency transport properties of beams or shells (Savin 2004, 2005a). This approach also yields Dirichlet and Neumann boundary conditions for the energy flux. Numerical simulations of the high-frequency energy propagation in a coupled system may be performed assuming that a transport regime holds in each substructure, and that the power flows at their junction are reflected and/or transmitted (with possible mode conversions) according to the laws derived above. This analysis neglects the waves guided by the interface, although a significant amount of energy may be transported by the latter. Note that Jin and Liao (2006) for example have adopted the same strategy for the computation of high-frequency elastic waves with an interface using the classical reflection/transmission coefficients between two semi-infinite elastic media.

The purpose of this paper is to expound a transport model for the high-frequency energy density in slender structures such as beams or shells, with due consideration of the energy fluxes between substructures. The objective of this research is to construct a general model of the high-frequency energy evolution within complex structures, in order to predict, for example, their steady-state or transient responses to broad-band excitations such as impact loads or shocks. The paper is organised as follows. First, the transport regime for the energy density associated to the high-frequency solution of a wave equation is recalled, as well as its adaptation to thick beams and shells. Then a system of coupled transport equations is introduced in section 3 in order to account for the energy transfers between two connected substructures. The coupling arises from the power flow boundary conditions at their interface. The derivation of power flow reflection/transmission coefficients by a wave component approach is detailed in section 4 for two coupled beams and two coupled plates. Some numerical simulations are presented and discussed in section 5. The final section of the paper offers a few conclusions.

2. Energy estimates and transport regime

In this section the basic results obtained in Akian (2003), Gérard *et al*. (1997), Guo and Wang (1999), Papanicolaou and Ryzhik (1999) for the transport properties of high-frequency waves in an isotropic, elastic medium are summarized. An energy estimator, namely the Wigner transform and its high-frequency limit, is introduced and its evolution properties are outlined. Then these results are specialized to beams and shells.

2.1 Notations and hypotheses

Let us consider an isotropic, elastic medium of density $\varrho(\mathbf{x}) > 0$ and elasticity tensor $\mathrm{C}(\mathbf{x})$. They both depend on the position $\mathbf{x}$ in the domain $\mathcal{O}$ (bounded or not) of $\mathbb{R}^d$ occupied by the elastic body, with $d = 1$, 2 or 3, and the elasticity tensor depends on two parameters solely. For small perturbations of its motion around a static equilibrium, its celerity $\mathbf{v}$ and stress fields $\boldsymbol{\sigma}$ are solutions of the homogeneous Navier equation:

$$\varrho\, \partial_t \mathbf{v} = \mathbf{Div}\boldsymbol{\sigma} \tag{1}$$

with the constitutive equation:

$$\partial_t \boldsymbol{\sigma}(\mathbf{x}, t) = \mathrm{C}(\mathbf{x})\boldsymbol{\varepsilon}(\mathbf{v}),\ \boldsymbol{\varepsilon}(\mathbf{v}) = \nabla_{\mathbf{x}} \otimes_s \mathbf{v} \tag{2}$$

Here $\boldsymbol{\varepsilon}$ stands for the linearized strain tensor, $\otimes_s$ is the symmetrized tensor product, $\nabla_{\mathbf{x}}$ is the gradient vector, and $t \in \mathbb{R}_+$ is the time variable. The associated mechanical energy density $\mathcal{E} \in \mathbb{R}_+$ and power flow density $\boldsymbol{\Pi} \in \mathbb{R}^d$ are given by:

$$\mathcal{E}(\mathbf{x}, t) = \frac{1}{2}\varrho|\mathbf{v}|^2 + \frac{1}{2}\boldsymbol{\sigma} : \boldsymbol{\varepsilon},\quad \boldsymbol{\Pi}(\mathbf{x}, t) = -\boldsymbol{\sigma}\mathbf{v} \tag{3}$$

where $|\mathbf{v}| = \sqrt{\mathbf{v} \cdot \bar{\mathbf{v}}}$, $\mathbf{u} \cdot \mathbf{v}$ is the euclidean scalar product of two vectors $\mathbf{u}$ and $\mathbf{v}$, $\bar{\mathbf{u}}$ is the complex conjugate of $\mathbf{u}$, $\mathbf{A} : \mathbf{B} = \mathrm{Tr}(\mathbf{A}\mathbf{B}^{\mathrm{T}})$ is the usual tensor scalar product, Tr is the trace of a matrix, and $\mathbf{A}^{\mathrm{T}}$ stands for the matrix transpose. High-frequency waves are considered introducing the rescaled variables $t \to \frac{t}{\varepsilon}$ and $\mathbf{x} \to \frac{\mathbf{x}}{\varepsilon}$, where ε is a small arbitrary parameter which is sent to 0 in the high-frequency limit, e.g., the wavelength. If $\mathbf{u} = (\mathbf{v}, \boldsymbol{\sigma})^{\mathrm{T}} \in \mathbb{C}^n$ is the state vector, then the constitutive and Navier Eq. (2) and (1), respectively, may be written as a generic system:

$$\varepsilon \partial_t \mathbf{u}_\varepsilon + P(\mathbf{x}, \varepsilon\mathrm{D})\mathbf{u}_\varepsilon = \mathbf{0},\quad \mathbf{x} \in \mathcal{O},\ t > 0 \tag{4}$$

where $\mathbf{u}_\varepsilon(\mathbf{x}, t) = \mathbf{u}\left(\frac{\mathbf{x}}{\varepsilon}, \frac{t}{\varepsilon}\right)$, and $P(\mathbf{x}, \mathrm{D})$ is a classical pseudo-differential operator on $\mathcal{S}(\mathbb{R}^d)$ (the Schwartz space of all $\mathcal{C}^\infty$ functions on $\mathbb{R}^d$ which are rapidly decreasing toward 0 at infinity as well as all their derivatives) of matrix-valued symbol $\mathbf{P}(\mathbf{x}, \mathbf{k})$. Here the standard form of the Fourier transform in $L^2(\mathbb{R}^d)$ is:

$$\hat{f}(\mathbf{k}) = \int_{\mathbb{R}^d} e^{-i\mathbf{k}\cdot\mathbf{x}} f(\mathbf{x})\mathrm{d}\mathbf{x},\quad f(\mathbf{x}) = \frac{1}{(2\pi)^d}\int_{\mathbb{R}^d} e^{i\mathbf{k}\cdot\mathbf{x}} \hat{f}(\mathbf{k})\mathrm{d}\mathbf{x}$$

$i = \sqrt{-1}$, and the pseudo-differential operator $K(\mathbf{x}, \mathrm{D})$ of symbol $\mathbf{K}(\mathbf{x}, \mathbf{k}) \in \mathcal{S}(T^*\mathbb{R}^d)$ (a smooth function of both arguments $\mathbf{x}$ and its dual variable $\mathbf{k} \in \mathbb{R}^d$) is:

$$K(\mathbf{x}, \varepsilon \mathrm{D}) f(\mathbf{x}) = \frac{1}{(2\pi)^d} \int_{\mathbb{R}^d} e^{\mathrm{i}\mathbf{k}\cdot\mathbf{x}} \mathbf{K}(\mathbf{x}, \varepsilon\mathbf{k}) \hat{f}(\mathbf{k}) \mathrm{d}\mathbf{x} \tag{5}$$

The phase space is $T^*\mathbb{R}^d \equiv \mathbb{R}^d_{\mathbf{x}} \times \mathbb{R}^d_{\mathbf{k}}$. Eqs. (1) and (2) for example yield:

$$P(\mathbf{x}, \mathrm{D}) = -\begin{pmatrix} 0 & \frac{1}{(\mathbf{x}\varrho} P_1(\mathrm{D}) \\ \mathrm{C}(\mathbf{x}) P_2(\mathrm{D}) & 0 \end{pmatrix}, \qquad P_1(\mathrm{D}) = \mathbf{Div}, \qquad P_2(\mathrm{D}) = \frac{1}{2}(\nabla + \nabla^{\mathrm{T}})$$

At last, "high frequencies" are initiated in the system of Eq. (4) by, say, "ε-oscillatory" initial conditions (Gérard *et al.* 1997) of the form:

$$\mathbf{u}_\varepsilon(\mathbf{x}, 0) = \mathbf{u}_0\left(\frac{\mathbf{x}}{\varepsilon}\right), \qquad \left\| \mathrm{D}\mathbf{u}_0 \right\|_{L^2} < \infty$$

2.2 Wigner transform, Wigner measure and transport properties

A Wigner transform of the state vector $\mathbf{u}_\varepsilon$ is considered in order to build up the corresponding high-frequency energy and power flow densities. The former is defined for two functions $\mathbf{u}_1$ and $\mathbf{u}_2$ in $\mathcal{S}'(\mathbb{R}^d)$, the set of temperate distributions on $\mathbb{R}^d$, by:

$$\mathbf{W}_\varepsilon[\mathbf{u}_1, \mathbf{u}_2](\mathbf{x}, \mathbf{k}) = \frac{1}{(2\pi)^d} \int_{\mathbb{R}^d} e^{\mathrm{i}\mathbf{k}\cdot\mathbf{y}} \mathbf{u}_1\left(\mathbf{x} - \frac{\varepsilon\mathbf{y}}{2}\right) \otimes \overline{\mathbf{u}_2\left(\mathbf{x} + \frac{\varepsilon\mathbf{y}}{2}\right)} \mathrm{d}\mathbf{y} \tag{6}$$

Provided that the sequence $(\mathbf{u}_\varepsilon)$ lies in a bounded subset of $L^2(\mathbb{R}^d)$, the complex $n \times n$ matrix-valued sequence $\mathbf{W}_\varepsilon(\mathbf{u}_\varepsilon) := \mathbf{W}_\varepsilon[\mathbf{u}_\varepsilon, \mathbf{u}_\varepsilon]$ has (up to an extracted subsequence) an Hermitian weak-* limit in $[\mathcal{S}'(T^*\mathbb{R}^d)]^{n,n}$ as $\varepsilon \to 0$ which is also a non-negative measure, the so-called Wigner measure $\mathbf{W}$ of $\mathbf{u}_\varepsilon$ (Gérard *et al.* 1997, Lions and Paul 1993). Furthermore, it satisfies:

$$\mathbf{PW} + \mathbf{WP}^* = \mathbf{0}$$

where $\mathbf{A}^*$ stands for the conjugate transpose. Therefore it writes:

$$\mathbf{W}(\mathbf{x}, \mathbf{k}, t) = \sum_{\alpha=1}^{M} \sum_{i,j=1}^{R_\alpha} \mathrm{w}_\alpha^{ij}(\mathbf{x}, \mathbf{k}, t) \mathbf{b}_{\alpha_j}(\mathbf{x}, \mathbf{k}) \otimes \mathbf{b}_{\alpha_i}(\mathbf{x}, \mathbf{k}) \tag{7}$$

where $\mathbf{b}_{\alpha_i}$ is the right eigenvector of the dispersion matrix $\mathbf{L} = -\mathrm{i}\mathbf{P}$ on $T^*\mathbb{R}^d \setminus \{(\mathbf{x}, \mathbf{k}); \mathbf{k} = 0\}$ associated to the eigenvalue $\lambda_\alpha(\mathbf{x}, \mathbf{k})$ of which order of multiplicity is R_α for an eigenmode α among the M existing ones, with $\mathrm{M} \le n$ and $\Sigma_{\alpha=1}^{M} R_\alpha = n$. R_α is assumed to be independent of $(\mathbf{x}, \mathbf{k})$. The left eigenvectors denoted by $\mathbf{c}_{\alpha_i}$ are normalized such that $\mathbf{b}_{\alpha_i} \cdot \mathbf{c}_{\beta_j} = \delta_{\alpha\beta}\delta_{ij}$, and one has $\mathrm{w}_\alpha^{ij} = \mathbf{W}\mathbf{c}_{\alpha_i} \cdot \mathbf{c}_{\alpha_j}$. These scalar coefficients are called phase-space energy densities, or specific intensities hereafter[2] The space-time energy density of

[2] The specific intensity, or radiance $L_\alpha(\mathbf{x}, t; |\mathbf{k}|, \hat{\mathbf{k}})$, is defined in the physical literature by:

$$L_\alpha(\mathbf{x}, t; |\mathbf{k}|, \hat{\mathbf{k}}) = |\mathbf{k}|^{d-1} \mathrm{w}_\alpha(\mathbf{x}, \mathbf{k}, \mathrm{t})$$

as a function of a unit vector $\hat{\mathbf{k}}$ on the unit sphere $\mathcal{S}^{d-1}$ of $\mathbb{R}^d$ and the wavenumber $|\mathbf{k}|$ in $\mathbb{R}_+$, such that $\mathbf{k} = |\mathbf{k}|\hat{\mathbf{k}}$. We will mix up both terminologies in this paper provided that no ambiguity holds.

the medium is then:

$$\mathcal{E}(\mathbf{x}, t) = \frac{1}{2} \sum_{\alpha=1}^{M} \sum_{i=1}^{R_\alpha} \int_{\mathbb{R}^d} \mathrm{w}_\alpha^{ii}(\mathbf{x}, \mathbf{k}, t) \mathrm{d}\mathbf{k} \tag{8}$$

and its space-time power flow density vector is given by:

$$\boldsymbol{\Pi}(\mathbf{x}, t) = \frac{1}{2} \sum_{\alpha=1}^{M} \sum_{i=1}^{R_\alpha} \int_{\mathbb{R}^d} \mathrm{w}_\alpha^{ii}(\mathbf{x}, \mathbf{k}, t) \nabla_{\mathbf{k}} \lambda_\alpha(\mathbf{x}, \mathbf{k}) \mathrm{d}\mathbf{k} \tag{9}$$

The $R_\alpha \times R_\alpha$ Wigner matrices $\mathbf{W}_\alpha$, with $W_{\alpha, ij} = \mathrm{w}_\alpha^{ij}$, are finally shown to satisfy the Liouville transport equations:

$$\partial_t \mathbf{W}_\alpha + \{\lambda_\alpha, \mathbf{W}_\alpha\} + \mathbf{W}_\alpha \mathbf{N}_\alpha - \mathbf{N}_\alpha \mathbf{W}_\alpha = \mathbf{0} \tag{10}$$

$\{f, g\} = \nabla_{\mathbf{k}} f \cdot \nabla_{\mathbf{x}} g - \nabla_{\mathbf{x}} f \cdot \nabla_{\mathbf{k}} g$ is the usual Poisson's bracket and $\mathbf{N}_\alpha$ is a skew-symmetric matrix with elements:

$$N_{\alpha, ij} = (\nabla_{\mathbf{k}} \mathbf{P} \cdot \nabla_{\mathbf{x}} \mathbf{b}_{\alpha_i} - \nabla_{\mathbf{x}} \lambda_\alpha \cdot \nabla_{\mathbf{k}} \mathbf{b}_{\alpha_i}) \cdot \mathbf{b}_{\alpha_j} - \frac{1}{2} (\nabla_{\mathbf{x}} \cdot \nabla_{\mathbf{k}} \lambda_\alpha) \delta_{ij} \tag{11}$$

The transport equations characterize the propagation of angularly resolved energy densities (the specific intensities) in $\mathcal{O}$ along rays defined by their wavenumber $|\mathbf{k}|$, direction $\hat{\mathbf{k}} = \mathbf{k}/|\mathbf{k}|$, and weight $\mathrm{Tr}\mathbf{W}_\alpha$ for a mode α among the M existing ones. The overall energy density (8) and power flow density (9) are reconstructed by a summation over all directions and wavenumbers. These results are adapted to elastic waves in slender structures or porous media in Savin (2004, 2005b, a), but they also apply to acoustic waves, electromagnetic waves, or the Schrödinger equation (Gérard *et al*. 1997, Guo and Wang 1999, Lions and Paul 1993, Papanicolaou and Ryzhik 1999). Visco-elastic media with memory effects have also been studied by Akian (2003).

2.3 Application to beams

The following results were given in Savin (2005a) for a thick beam (Timoshenko kinematics) of which deflection is denoted by w, axial motion by u, and section bending angle by θ. Let $R(x)$ be its radius of curvature, $\varrho(x)$ be its mass per unit length, $E(x)$ its Young's modulus, $\kappa G(x)$ its reduced shear modulus, where κ is the usual shear reduction factor depending on the cross-section geometry and Poisson's coefficient, and $r(x) = \sqrt{I/S}$ its radius of gyration where I and S are respectively the cross-section inertia and area. The axial force N, shear force T, and bending moment M are given by:

$$N = ES\left(\partial_x u + \frac{w}{R}\right), \quad T = \kappa GS\left(\partial_x w - \theta - \frac{u}{R}\right), \quad M = EI\partial_x \theta \tag{12}$$

where x is the curvilinear abscissa along the beam. The equations of motion are:

$$\varrho\partial_t^2 u = \partial_x N + \frac{T}{R}, \quad \varrho\partial_t^2 w = \partial_x T - \frac{N}{R}, \quad \varrho r^2 \partial_t^2 \theta = T + \partial_x M \tag{13}$$

Let $\mathbf{u} = (\partial_t u, \partial_t w, \partial_t \theta, N, T, M)^{\mathrm{T}}$, then Eqs. (12) and (13) are written as a system (4) with $d = 1$, $n = 6$, and $\mathbf{P}(x, k) = \mathrm{i}\mathbf{L}(x, k) + \mathbf{\Omega}(x)$, where:

$$-\mathbf{L} = k\mathbf{M}^{-1}\begin{bmatrix} 0 & \mathbb{I}_3 \\ \mathbb{I}_3 & 0 \end{bmatrix}, \quad \mathbf{\Omega} = \mathbf{M}^{-1}\begin{bmatrix} 0 & \mathbf{\Omega}_3 \\ -\mathbf{\Omega}_3^{\mathrm{T}} & 0 \end{bmatrix} \tag{14}$$

and:

$$\mathbf{\Omega}_3 = \begin{bmatrix} 0 & -\frac{1}{R} & 0 \\ \frac{1}{R} & 0 & 0 \\ 0 & -1 & 0 \end{bmatrix}, \quad \mathbf{M} = \mathrm{diag}\left\{\varrho, \varrho, \varrho r^2, \frac{1}{ES}, \frac{1}{\kappa GS}, \frac{1}{EI}\right\}$$

Throughout the paper $\mathbb{I}_j$ is the $j \times j$ identity matrix. The eigenvalues of the dispersion matrix $\mathbf{L}$ for $k \neq 0$ are given by:

$$\begin{aligned} \lambda_{\mathrm{T}}^{\pm} &= \pm c_{\mathrm{T}}|k| \text{ each with multiplicity 1} \\ \lambda_{\mathrm{P}}^{\pm} &= \pm c_{\mathrm{P}}|k| \text{ each with multiplicity 2} \end{aligned} \tag{15}$$

where $c_{\mathrm{T}} = \sqrt{\frac{\kappa GS}{\varrho}}$, $c_{\mathrm{P}} = \sqrt{\frac{ES}{\varrho}}$ and the associated eigenvectors are:

$$\begin{aligned} \mathbf{b}_{\mathrm{T}}^{\pm} &= \left(0, \frac{\mathrm{sign}(k)}{\sqrt{2\varrho}}, 0, 0, \mp\sqrt{\frac{\kappa Gh}{2}}, 0\right)^{\mathrm{T}} \\ \mathbf{b}_{\mathrm{Pb}}^{\pm} &= \left(0, 0, \frac{\mathrm{sign}(k)}{\sqrt{2\varrho r^2}}, 0, 0, \mp\sqrt{\frac{EI}{2}}\right)^{\mathrm{T}} \\ \mathbf{b}_{\mathrm{Pn}}^{\pm} &= \left(\frac{\mathrm{sign}(k)}{\sqrt{2\varrho}}, 0, 0, \mp\sqrt{\frac{ES}{2}}, 0, 0\right)^{\mathrm{T}} \end{aligned} \tag{16}$$

Mode T corresponds to the transverse shear energy, and the coupled modes P correspond to the compressional and bending energies. Let $\mathbf{W}_{\mathrm{P}}^{\pm}(x, k, t)$ be the 2×2 Wigner matrices of specific intensities for the axial and bending waves corresponding to eigenvectors $\mathbf{b}_{\mathrm{Pb}}^{\pm}(x, k)$ and $\mathbf{b}_{\mathrm{Pn}}^{\pm}(x, k)$. Then they satisfy the following transport equations:

$$\partial_t \mathbf{W}_{\mathrm{P}}^{\pm} \pm \mathrm{sign}(k) c_{\mathrm{P}} \partial_x \mathbf{W}_{\mathrm{P}}^{\pm} \mp |k| \partial_x c_{\mathrm{P}} \partial_k \mathbf{W}_{\mathrm{P}}^{\pm} = \mathbf{0} \tag{17}$$

since the rotation matrices $\mathbf{N}_{\mathrm{P}}^{\pm}(x, k)$ as given by Eq. (11) are null for a beam. As regards the transverse waves, specific intensities $\mathrm{w}_{\mathrm{T}}^{\pm}(x, k, t)$ satisfy the equations:

$$\partial_t \mathrm{w}_{\mathrm{T}}^{\pm} \pm \mathrm{sign}(k) c_{\mathrm{T}} \partial_x \mathrm{w}_{\mathrm{T}}^{\pm} \mp |k| \partial_x c_{\mathrm{T}} \partial_k \mathrm{w}_{\mathrm{T}}^{\pm} = 0 \tag{18}$$

and they are uncoupled from the P modes. Observe that necessarily $w_T^-(x, k, t) = w_T^+(x, -k, t)$ and $\mathbf{W}_P^-(x, k, t) = \mathbf{W}_P^+(x, -k, t)$, so that the energy density of the beam is estimated by:

$$\mathcal{E}(x, t) = \int_{\mathbb{R}} w_T^+(x, k, t)\mathrm{d}k + \int_{\mathbb{R}} \mathrm{Tr}\mathbf{W}_P^+(x, k, t)\mathrm{d}k \tag{19}$$

while the power flow density is estimated by:

$$\begin{aligned}\Pi(x, t) &= c_T(x)\int_0^{+\infty}(w_T^+(x, k, t) + w_T^-(x, k, t))\mathrm{d}k \\ &+ c_P(x)\int_0^{+\infty}\mathrm{Tr}(\mathbf{W}_P^+(x, k, t) + \mathbf{W}_P^-(x, k, t))\mathrm{d}k\end{aligned} \tag{20}$$

2.4 Application to shells

The following results were derived in Savin (2004). Let us consider a thick curved shell $\Sigma \times (-h/2, h/2)$ of which vibrations are described by the model of Naghdi and Cooper (1956). The (regular) middle surface Σ is parametrized by its curvilinear coordinates $\mathbf{x} = (x_1, x_2)^T$ and its gradient vector is $\nabla_\Sigma := (\partial_1, \partial_2)^T$; thus $d = 2$ with the notations of section 2.1. The associated natural tangent basis is denoted by $(\mathbf{e}_1, \mathbf{e}_2)$ such that $\mathbf{e}_1 = \partial_1 \mathbf{x}$ and $\mathbf{e}_2 = \partial_2 \mathbf{x}$. The tangent motions of the middle surface are denoted by $\mathbf{u}_\Sigma$, w is the normal displacement, and $\boldsymbol{\theta}$ is the vector of changes of slope of the unit normal $\hat{\mathbf{n}} = (\mathrm{e}_1 \times \mathrm{e}_2) / (|\mathrm{e}_1 \times \mathrm{e}_2|)$ to Σ; see Fig. (1). The second-order, normal curvature tensor $\mathbb{B}$ of the shell is:

$$\mathbb{B} = \sum_{\alpha, \beta = 1}^{2} B_{\alpha\beta}\mathbf{e}_\alpha \otimes \mathbf{e}_\beta, \quad B_{\alpha\beta} = -\mathbf{e}_\alpha \cdot \partial_\beta \hat{\mathbf{n}} = \hat{\mathbf{n}} \cdot \partial_\beta \mathbf{e}_\alpha$$

and it is symmetric. Its inverse trace $(\mathrm{Tr}\mathbb{B})^{-1}$, the mean radius of the shell at each point of Σ, is assumed to be much larger than the thickness h, which in turn is significantly lower than a typical wavelength of the excitations.

Let $\varrho(\mathbf{x})$ be the mass per unit surface of the isotropic material constituting the shell and let C be its fourth-order elasticity tensor. Let $E(\mathbf{x})$ be its Young's modulus, $G(\mathbf{x})$ its shear modulus such that $G = \dfrac{E}{2(1 + \nu)}$, $\kappa < 1$ its shear reduction coefficient and ν its Poisson's coefficient. The constitutive equation is written:

$$\mathrm{C}:\boldsymbol{\varepsilon} = \frac{\nu E}{1 - \nu^2}(\mathrm{Tr}\boldsymbol{\varepsilon})\mathbb{I}_d + \frac{E}{1 + \nu}\boldsymbol{\varepsilon}$$

for the second-order linearized strain tensor $\boldsymbol{\varepsilon}$, and the membrane forces tensor $\mathbb{N}$, shear forces $\mathbf{T}$ and bending moments tensor $\mathbb{M}$ are given by:

$$\begin{aligned}\mathbb{N} &= h\mathrm{C}:(\nabla_\Sigma \otimes_s \mathbf{u}_\Sigma - w\mathbb{B}) \\ \mathbf{T} &= \kappa G h(\nabla_\Sigma w - \boldsymbol{\theta} - \mathbb{B}\mathbf{u}_\Sigma) \\ \mathbb{M} &= \frac{h^3}{12}\mathrm{C}:\nabla_\Sigma \otimes_s \boldsymbol{\theta}\end{aligned} \tag{21}$$

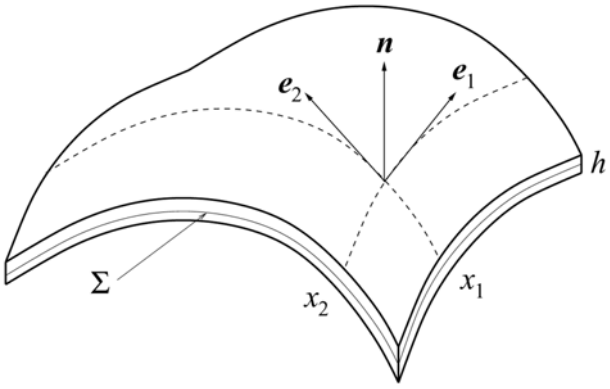

Fig. 1 An elastic shell structure occupying the domain $\Sigma \times (-h/2,\ h/2)$ of $\mathbb{R}^3$. Σ is the middle surface of the shell, h is its thickness and $(\mathbf{e}_1,\ \mathbf{e}_2)$ is its natural tangent basis at the point $\mathbf{x} = (x_1,\ x_2)$. $\hat{\mathbf{n}}$ is the unit mormal outward to the middle surface.

The equations of motion are:

$$\begin{aligned} \varrho \partial_t^2 \mathbf{u}_\Sigma &= \mathbf{Div}_\Sigma \mathbb{N} + \mathbb{B}\mathbf{T} \\ \varrho \partial_t^2 w &= \mathrm{div}_\Sigma \mathbf{T} + \mathbb{B} : \mathbb{N} \\ \frac{\varrho h^2}{12} \partial_t^2 \boldsymbol{\theta} &= \mathbf{Div}_\Sigma \mathbb{M} + \mathbf{T} \end{aligned} \tag{22}$$

Let $\mathbf{u} = (\partial_t \mathbf{u}_\Sigma,\ \partial_t w,\ \partial_t \boldsymbol{\theta},\ \mathbf{N},\ \mathbf{T},\ \mathbf{M})^{\mathrm{T}}$, where $\mathbf{N}$ and $\mathbf{M}$ are the three-component vector counterparts of $\mathbb{N}$ and $\mathbb{M}$, respectively, which are symmetric. For the model of Naghdi and Cooper considered in this analysis, the normal curvature tensor is $\mathbb{B} = -\frac{1}{R}\mathbf{e}_2 \otimes \mathbf{e}_2$ if R is the radius of the circular cylindrical shell. Then Eqs. (21)-(22) are equivalent to the system (4) for $n = 13$ and $\mathbf{P}(\mathbf{x},\ \mathbf{k}) = \mathrm{i}\mathbf{L}(\mathbf{x},\ \mathbf{k}) + \boldsymbol{\Omega}(\mathbf{x})$, where:

$$-\mathbf{L} = \begin{bmatrix} 0 & 0 & 0 & \frac{1}{\varrho}\mathbf{K}(\mathbf{k}) & \frac{1}{\varrho}\mathbf{m}(\mathbf{k}) & 0 & 0 & 0 \\ 0 & 0 & 0 & 0 & 0 & \frac{1}{\varrho}\mathbf{k}^{\mathrm{T}} & 0 & 0 \\ 0 & 0 & 0 & 0 & 0 & 0 & \frac{h}{\varrho I}\mathrm{K}(\mathbf{k}) & \frac{h}{\varrho I}\mathbf{m}(\mathbf{k}) \\ C\mathbf{A}\mathbf{K}(\mathbf{k}) & 0 & 0 & 0 & 0 & 0 & 0 & 0 \\ Gh\mathbf{m}(\mathbf{k})^{\mathrm{T}} & 0 & 0 & 0 & 0 & 0 & 0 & 0 \\ 0 & \kappa Gh\mathbf{k} & 0 & 0 & 0 & 0 & 0 & 0 \\ 0 & 0 & D\mathbf{A}\mathbf{K}(\mathbf{k}) & 0 & 0 & 0 & 0 & 0 \\ 0 & 0 & GI\mathbf{m}(\mathbf{k})^{\mathrm{T}} & 0 & 0 & 0 & 0 & 0 \end{bmatrix} \tag{23}$$

with:

$$\mathbf{A} = \begin{bmatrix} 1 & \nu \\ \nu & 1 \end{bmatrix}, \quad C = \frac{Eh}{1-\nu^2}, \quad D = \frac{EI}{1-\nu^2}, \quad I = \frac{h^3}{12}$$

and $\mathbf{k} = (k_1, k_2)^{\mathrm{T}}$, $\mathbf{K}(\mathbf{k}) = \mathrm{diag}\ \{k_1, k_2\}$, $\mathbf{m}(\mathbf{k}) = (k_2, k_1)^{\mathrm{T}}$. The skew-symmetric matrix $\boldsymbol{\Omega}$ is given by:

$$-\boldsymbol{\Omega} = \mathbf{M}^{-1} \begin{bmatrix} 0 & 0 & 0 & 0 & 0 & \mathbb{B} & 0 & 0 \\ & 0 & 0 & \mathbf{r} & 0 & 0 & 0 & 0 \\ & & 0 & 0 & 0 & \mathbb{I}_2 & 0 & 0 \\ & & & 0 & 0 & 0 & 0 & 0 \\ & & & & 0 & 0 & 0 & 0 \\ & & & & & 0 & 0 & 0 \\ & & & & & & 0 & 0 \\ & & & & & & & 0 \end{bmatrix}$$

with $\mathbf{r} = (0, -\mathrm{Tr}\mathbb{B})$ and:

$$\mathbf{M}(\mathbf{x}) = \mathrm{diag}\left\{\varrho\,\mathbb{I}_2, \varrho, \frac{\varrho I}{h}\mathbb{I}_2, (C\mathbf{A})^{-1}, \frac{1}{Gh}, \frac{1}{\kappa Gh}\,\mathbb{I}_2, (D\mathbf{A})^{-1}, \frac{1}{GI}\right\}$$

Let $|\mathbf{k}| = \sqrt{k_1^2 + k_2^2}$, $\hat{\mathbf{k}} = \frac{1}{|\mathbf{k}|}(k_1, k_2)^{\mathrm{T}}$ and $\hat{\mathbf{I}} = \frac{1}{|\mathbf{k}|}(-k_2, k_1)^{\mathrm{T}}$. Then the eigenvalues of the dispersion matrix $\mathbf{L}$ on the set $\mathcal{A} = T^*\mathbb{R}^2 \setminus \{(\mathbf{x}, \mathbf{k});\ \mathbf{k} = \mathbf{0}\}$ are:

$$\begin{aligned} \lambda_0 &= 0 \text{ with multiplicity 3} \\ \lambda_{\mathrm{T}}^{\pm} &= \pm c_{\mathrm{T}}|\mathbf{k}| \text{ each with multiplicity 1} \\ \lambda_{\mathrm{S}}^{\pm} &= \pm c_{\mathrm{S}}|\mathbf{k}| \text{ each with multiplicity 2} \\ \lambda_{\mathrm{P}}^{\pm} &= \pm c_{\mathrm{P}}|\mathbf{k}| \text{ each with multiplicity 2} \end{aligned} \tag{24}$$

with $c_{\mathrm{S}} = \sqrt{\frac{Gh}{\varrho}}$, $c_{\mathrm{T}} = \sqrt{\kappa} c_{\mathrm{S}}$ and $c_{\mathrm{P}} = \sqrt{\frac{C}{\varrho}}$, and the associated eigenvectors on $\mathcal{A}$ are:

$$\mathbf{b}_{1,2} = \left(0, 0, 0, 0, 0, \pm\sqrt{\frac{\kappa Gh}{2}}\hat{\mathbf{I}}, \sqrt{\frac{EI}{2}}\mathbf{K}(\hat{\mathbf{I}})\hat{\mathbf{I}}, \frac{1}{2}\sqrt{\frac{EI}{2}}\mathbf{m}(\hat{\mathbf{I}}) \cdot \hat{\mathbf{I}}\right)^{\mathrm{T}}$$

$$\mathbf{b}_3 = \left(0, 0, 0, \sqrt{Eh}\mathbf{K}(\hat{\mathbf{I}})\hat{\mathbf{I}}, \frac{1}{2}\sqrt{Eh}\mathbf{m}(\hat{\mathbf{I}}) \cdot \hat{\mathbf{I}}, 0, 0, 0\right)^{\mathrm{T}}$$

$$\mathbf{b}_{\mathrm{T}}^{\pm} = \left(0, \frac{1}{\sqrt{2\varrho}}, 0, 0, 0, \mp\sqrt{\frac{\kappa Gh}{2}}\hat{\mathbf{k}}, 0, 0\right)^{\mathrm{T}}$$

$$\mathbf{b}_{\mathrm{Sb}}^{\pm} = \left(0, 0, \mp\sqrt{\frac{h}{2\varrho I}}\hat{\mathbf{I}}, 0, 0, 0, \sqrt{(1-\nu)D}\mathbf{K}(\hat{\mathbf{k}})\hat{\mathbf{I}}, \frac{1}{2}\sqrt{2GI}\mathbf{m}(\hat{\mathbf{k}}) \cdot \hat{\mathbf{I}}\right)^{\mathrm{T}}$$

$$\mathbf{b}^{\pm}_{\mathrm{Sn}} = \left(\pm\frac{h}{\sqrt{2\varrho}}\hat{\mathbf{I}},\, 0,\, 0,\, \sqrt{(1-\nu)C}\,\mathbf{K}(\hat{\mathbf{k}})\hat{\mathbf{I}},\, \frac{1}{2}\sqrt{2Gh}\,\mathbf{m}(\hat{\mathbf{k}})\cdot\hat{\mathbf{I}},\, 0,\, 0,\, 0\right)^{\mathrm{T}}$$

$$\mathbf{b}^{\pm}_{\mathrm{Pb}} = \left(0,\, 0,\, \mp\sqrt{\frac{h}{2\varrho I}}\hat{\mathbf{k}},\, 0,\, 0,\, 0,\, \sqrt{\frac{D}{2}}\mathbf{A}\,\mathbf{K}(\hat{\mathbf{k}})\hat{\mathbf{k}},\, \frac{1}{2}\sqrt{(1-\nu)GI}\,\mathbf{m}(\hat{\mathbf{k}})\cdot\hat{\mathbf{k}}\right)^{\mathrm{T}}$$

$$\mathbf{b}^{\pm}_{\mathrm{Pn}} = \left(\pm\frac{1}{\sqrt{2\varrho}}\hat{\mathbf{k}},\, 0,\, 0,\, \sqrt{\frac{C}{2}}\mathbf{A}\,\mathbf{K}(\hat{\mathbf{k}})\hat{\mathbf{k}},\, \frac{1}{2}\sqrt{(1-\nu)Gh}\,\mathbf{m}(\hat{\mathbf{k}})\cdot\hat{\mathbf{k}},\, 0,\, 0,\, 0\right)^{\mathrm{T}} \tag{25}$$

Modes 0 are non-propagative vortical modes, the mode T corresponds to a pure transverse shear energy, and the coupled modes P and S correspond to in-plane and bending energies. Given the projection (7) of the Wigner measure (on $\mathcal{A}$), let $\mathbf{W}^{\pm}_{\mathrm{P}}(\mathbf{x},\, \mathbf{k},\, t)$ be the 2×2 Wigner matrices of specific intensities for bending and in-plane waves corresponding to eigenvectors $\mathbf{b}^{\pm}_{\mathrm{Pb}}(\mathbf{x},\, \mathbf{k})$ and $\mathbf{b}^{\pm}_{\mathrm{Pn}}(\mathbf{x},\, \mathbf{k})$. Similarly, let $\mathbf{W}^{\pm}_{\mathrm{S}}(\mathbf{x},\, \mathbf{k},\, t)$ be the 2×2 Wigner matrices of specific intensities corresponding to eigenvectors $\mathbf{b}^{\pm}_{\mathrm{Sb}}(\mathbf{x},\, \mathbf{k})$ and $\mathbf{b}^{\pm}_{\mathrm{Sn}}(\mathbf{x},\, \mathbf{k})$. Then they satisfy the following transport equations:

$$\partial_t \mathbf{W}^{\pm}_{\alpha} \pm c_{\alpha}\hat{\mathbf{k}}\cdot\nabla_{\mathbf{x}}\mathbf{W}^{\pm}_{\alpha} \mp |\mathbf{k}|\nabla_{\mathbf{x}}c_{\alpha}\cdot\nabla_{\mathbf{x}}\mathbf{W}^{\pm}_{\alpha} = \mathbf{0}, \quad \alpha = \mathrm{P},\, \mathrm{S} \tag{26}$$

since rotation matrices $\mathbf{N}^{\pm}_{\mathrm{P}}(\mathbf{x},\, \mathbf{k})$ and $\mathbf{N}^{\pm}_{\mathrm{S}}(\mathbf{x},\, \mathbf{k})$ as given by Eq. (11) are null for the present case. As regards shear waves, specific intensities $\mathrm{w}^{\pm}_{\mathrm{T}}(\mathbf{x},\, \mathbf{k},\, t)$ satisfy the equations:

$$\partial_t \mathrm{w}^{\pm}_{\mathrm{T}} \pm c_{\mathrm{T}}\hat{\mathbf{k}}\cdot\nabla_{\mathbf{x}}\mathrm{w}^{\pm}_{\mathrm{T}} \mp |\mathbf{k}|\nabla_{\mathbf{x}}c_{\mathrm{T}}\cdot\nabla_{\mathbf{x}}\mathrm{w}^{\pm}_{\mathrm{T}} = 0 \tag{27}$$

and they are uncoupled from the bending modes. At last the 3×3 Wigner matrix $\mathbf{W}_0(\mathbf{x},\, \mathbf{k},\, t)$ satisfies:

$$\partial_t \mathbf{W}_0 = \mathbf{0} \tag{28}$$

since here, again, $\mathbf{N}_0 = \mathbf{0}$; thus $\mathbf{W}_0(\mathbf{x},\, \mathbf{k},\, t) = \mathbf{0}$ if it is initially null. As for beams we observe that $\mathrm{w}^{-}_{\mathrm{T}}(\mathbf{x},\, \mathbf{k},\, t) = \mathrm{w}^{+}_{\mathrm{T}}(\mathbf{x},\, -\mathbf{k},\, t)$ and $\mathbf{W}^{-}_{\alpha}(\mathbf{x},\, \mathbf{k},\, t) = \mathbf{W}^{+}_{\alpha}(\mathbf{x},\, -\mathbf{k},\, t)$ for $\alpha = \mathrm{S}$ or P, so that the energy density is estimated by:

$$\mathcal{E}(\mathbf{x},\, t) = \int_{\mathbb{R}^2} \mathrm{w}^{+}_{\mathrm{T}}(\mathbf{x},\, \mathbf{k},\, t)\mathrm{d}\mathbf{k} + \sum_{\alpha=\mathrm{S},\,\mathrm{P}} \int_{\mathbb{R}^2} \mathrm{Tr}\,\mathbf{W}^{+}_{\alpha}(\mathbf{x},\, \mathbf{k},\, t)\mathrm{d}\mathbf{k} \tag{29}$$

while the power flow density vector is estimated by:

$$\Pi(\mathbf{x},\, t) = c_{\mathrm{T}}(\mathbf{x})\int_{\mathbb{R}^2} \mathrm{w}^{+}_{\mathrm{T}}(\mathbf{x},\, \mathbf{k},\, t)\hat{\mathbf{k}}\mathrm{d}\mathbf{k} + \sum_{\alpha=\mathrm{S},\,\mathrm{P}} c_{\alpha}(\mathbf{x})\int_{\mathbb{R}^2} \mathrm{Tr}\,\mathbf{W}^{+}_{\alpha}(\mathbf{x},\, \mathbf{k},\, t)\hat{\mathbf{k}}\mathrm{d}\mathbf{k} \tag{30}$$

The energy rays $\tau \to \mathbf{x}_{\alpha}(\tau)$ for each mode α are characterized by their tangent vector $\mathrm{D}_{\tau}\mathbf{x}_{\alpha} = c_{\alpha}\mathbf{t}$ with $|\mathrm{D}_{\tau}\mathbf{x}_{\alpha}| = 1$ and $\mathrm{D}_{\tau}\mathbf{t} = -|\mathbf{t}|\nabla_{\Sigma}c_{\alpha}$; after eliminating $\mathbf{t}$, a generalized Snell-Descartes law is obtained in the form:

$$\frac{\mathrm{d}}{\mathrm{d}\tau}\left(\frac{1}{c_{\alpha}}\frac{\mathrm{d}\mathbf{x}_{\alpha}}{\mathrm{d}\tau}\right) = \nabla_{\Sigma}\left(\frac{1}{c_{\alpha}}\right) \tag{31}$$

In the case of an homogeneous material where c_{α} is independent of position $\mathbf{x}$, the above equation shows that the rays are the geodesic lines of the shell. Finally the time τ_{12} needed by the energy density to travel the rays from a point $\mathbf{x}_1$ to a point $\mathbf{x}_2$ is given by $\tau_{12} = \int_{\mathbf{x}_1}^{\mathbf{x}_2} |\mathbf{t}|\mathrm{d}\mathbf{x}$.

3. Energy transport in coupled structures

The derivation of section 2 is used to model the high-frequency energy flows in coupled structures by the transport theory. Firstly, one considers that the transport regime holds in each substructure. Then the power flows in each of them are reflected/transmitted by their interfaces assuming that the reflection/transmission efficiencies are known operators. In a subsequent section 4, we show how to formally compute these operators for coupled beams or plates by a dedicated analysis which is coherent with the transport characteristics of such structures.

Let us consider two substructures which occupy the domains $\mathcal{O}_1$ and $\mathcal{O}_2$ of $\mathbb{R}^d$ such that their junction $\partial\mathcal{O}_1 \cap \partial\mathcal{O}_2 = \Gamma$ is a smooth manifold of codimension 1 of which outward unit normal with respect to $\mathcal{O}_r$, $r = 1, 2$, is denoted by $\hat{\mathbf{n}}^r(\mathbf{x}), \mathbf{x} \in \Gamma$, with $\hat{\mathbf{n}}^1(\mathbf{x}) = -\hat{\mathbf{n}}^2(\mathbf{x})$. Let $P_{\mathbf{x}} = \mathbb{I}_d - \hat{\mathbf{n}}^1 \otimes \hat{\mathbf{n}}^1 = \mathbb{I}_d - \hat{\mathbf{n}}^2 \otimes \hat{\mathbf{n}}^2$ be the orthogonal projection on the tangent space $T_{\mathbf{x}}\Gamma$ at $\mathbf{x}$. We introduce the notation $\mathbf{k}' = P_{\mathbf{x}}\mathbf{k}$ for $\mathbf{k} \in \mathbb{R}^d$ or $\hat{\mathbf{k}}' = P_{\mathbf{x}}\hat{\mathbf{k}}$ for $\hat{\mathbf{k}} \in \mathcal{S}^{d-1}$. The transport theory outlined in the previous section holds in the interior of each subsystem. The transport equations are then Eq. (10):

$$\partial_t \mathbf{W}^r_\alpha + \{\lambda^r_\alpha, \mathbf{W}^r_\alpha\} + \mathbf{W}^r_\alpha \mathbf{N}^r_\alpha - \mathbf{N}^r_\alpha \mathbf{W}^r_\alpha = \mathbf{0}, \quad r = 1, 2 \tag{32}$$

written for each substructure. We assume that their eigenvalues (Hamiltonians) are $\lambda^r_\alpha(\mathbf{x}, \mathbf{k}) = c^r_\alpha(\mathbf{x})|\mathbf{k}|$, in accordance with the results obtained in sections 2.3 and 2.4. As in classical mechanics, the Hamiltonians remain constant along the energy rays, even when they are reflected or transmitted by an interface (Bal *et al.* 1999, Jin and Liao 2006) or diffracted by some random heterogeneities (Guo and Wang 1999, Papanicolaou and Ryzhik 1999, Savin 2004, 2005b). Thus:

$$c^r_\alpha(\mathbf{x})\left|\mathbf{k}^r_\alpha\right| = c^s_\beta(\mathbf{x})\left|\mathbf{k}^s_\beta\right| := \omega, \quad \mathbf{x} \in \Gamma \tag{33}$$

whenever $r, s = 1, 2$ and $1 \le \alpha \le M_r$, $1 \le \beta \le M_s$ where M_r is the number of energy modes in subsystem r. The traces of the wave speeds c^r_α on Γ are defined by $c^r_\alpha(\mathbf{x}) := \lim_{h \to 0} c^r_\alpha(\mathbf{x} - h\hat{\mathbf{n}}^r)$, $\mathbf{x} \in \Gamma$. The condition (33) holds for either reflected ($r = s$) or transmitted ($r \neq s$) energy rays and can be used to determine the reflected and transmitted wavenumbers $\left|\mathbf{k}^r_\alpha\right|$ from either side of the interface given an incident wave vector $\mathbf{k}$. Also the tangent wave vector $\mathbf{k}'$ is constant across the junction: $\mathbf{k}' = P_{\mathbf{x}}\mathbf{k} = P_{\mathbf{x}}\mathbf{k}^r_\alpha$ for $r = 1$ or 2 and $1 \le \alpha \le M_r$, owing to Snell-Descartes law. The normal wavenumbers χ^r_α on the interface from $\mathcal{O}_r$, $r = 1, 2$, are defined by $\chi^r_\alpha(\mathbf{k}') = \left|\mathbf{k}^r_\alpha\right|\hat{\chi}^r_\alpha(\mathbf{k}') = \mathbf{k}^r_\alpha \cdot \hat{\mathbf{n}}^r$, such that $\mathbf{k}^r_\alpha = \mathbf{k}' + \chi^r_\alpha \hat{\mathbf{n}}^r$ for the wave vector of a mode α in $\mathcal{O}_r$, with:

$$\chi^r_\alpha(\mathbf{k}') = \pm\sqrt{\left(\frac{\omega}{c^r_\alpha}\right)^2 - |\mathbf{k}'|^2}$$

Here $\omega(\mathbf{k}')$ is the constant in Eq. (33) for a given incident wave vector $\mathbf{k}$. We consider only propagating waves because the energy in evanescent waves is exponentially small away from the boundary. Therefore we assume above that the normal wavenumbers χ^r_α are real and the support of $\mathbf{W}^r_\alpha$ is uniformly inside the ball $\{|\mathbf{k}'| < \omega / c^r_\alpha\}$. Then the transported energy in $\mathcal{O}_1$ flowing away from the boundary after reflection and transmission is written (see for example Bal *et al.* 1999):

$$c^1_\alpha(\mathbf{x})\left|\hat{\chi}^1_\alpha(\mathbf{k}')\right|(\mathrm{w}^{ii}_\alpha)^1(\mathbf{x}, \mathbf{k}', -\chi^1_\alpha, t) =$$
$$\sum_{\beta=1}^{M_1}\sum_{j=1}^{R^1_\beta} c^1_\beta(\mathbf{x})\left|\hat{\chi}^1_\beta(\mathbf{k}')\right|\rho^{11}_{\alpha_i\beta_j}(\mathbf{x}, \mathbf{k}')(\mathrm{w}^{jj}_\beta)^1(\mathbf{x}, \mathbf{k}', \chi^1_\beta, t)$$

$$+\sum_{\beta=1}^{M_2}\sum_{j=1}^{R_\beta^2} c_\beta^2(\mathbf{x})\left|\hat{\chi}_\beta^2(\mathbf{k}')\right| \tau_{\alpha_i\beta_j}^{12}(\mathbf{x},\mathbf{k}')(\mathrm{w}_\beta^{jj})^2(\mathbf{x},\mathbf{k}',\chi_\beta^2,t) \quad \text{on } T\Gamma \tag{34}$$

and the transported energy in $\mathcal{O}_2$ flowing away from the boundary is:

$$\begin{aligned} & c_\alpha^2(\mathbf{x})\left|\hat{\chi}_\alpha^2(\mathbf{k}')\right|(\mathrm{w}_\alpha^{ii})^2(\mathbf{x},\mathbf{k}',-\chi_\alpha^2,t) = \\ & \sum_{\beta=1}^{M_2}\sum_{j=1}^{R_\beta^2} c_\beta^2(\mathbf{x})\left|\hat{\chi}_\beta^2(\mathbf{k}')\right|\rho_{\alpha_i\beta_j}^{22}(\mathbf{x},\mathbf{k}')(\mathrm{w}_\beta^{jj})^2(\mathbf{x},\mathbf{k}',\chi_\beta^2,t) \\ & +\sum_{\beta=1}^{M_1}\sum_{j=1}^{R_\beta^1} c_\beta^1(\mathbf{x})\left|\hat{\chi}_\beta^1(\mathbf{k}')\right| \tau_{\alpha_i\beta_j}^{21}(\mathbf{x},\mathbf{k}')(\mathrm{w}_\beta^{jj})^1(\mathbf{x},\mathbf{k}',\chi_\beta^1,t) \quad \text{on } T\Gamma \end{aligned} \tag{35}$$

where $T\Gamma$ is the tangent bundle of Γ. $\rho_{\alpha_i\beta_j}^{rr}$ is the power flow reflection coefficient in $\mathcal{O}_r$ for the conversion of an incident ray in the eigenmode β_j into a reflected ray in the eigenmode α_i, and $\tau_{\alpha_i\beta_j}^{rs}$ is the power flow transmission coefficient for the conversion of an incident ray in the eigenmode β_j in $\mathcal{O}_s$ into a transmitted ray in the eigenmode α_i in $\mathcal{O}_r$, $r \neq s$. In the next section, we show how to compute them for coupled beams or plates. They shall satisfy the following energy flux conservation law:

$$\sum_{\alpha=1}^{M_r}\sum_{i=1}^{R_\alpha^r}\frac{c_\alpha^r\left|\hat{\chi}_\alpha^r\right|}{c_\beta^r\left|\hat{\chi}_\beta^r\right|}\rho_{\alpha_i\beta_j}^{rr} + \sum_{\alpha=1}^{M_s}\sum_{i=1}^{R_\alpha^s}\frac{c_\alpha^s\left|\hat{\chi}_\alpha^s\right|}{c_\beta^r\left|\hat{\chi}_\beta^r\right|}\tau_{\alpha_i\beta_j}^{sr} \leq 1, \quad s \neq r \tag{36}$$

where the equality holds for a lossless interface. This equation states that the total flux impinging the junction in a given eigenmode is either reflected or transmitted, with or without losses. In the following we consider only conservative interfaces. The glancing region where $\hat{\mathbf{k}} \cdot \hat{\mathbf{n}}^r = 0$ is also neglected in the above formulation, not because gliding rays (those which are possibly trapped by a non-convex interface) are unlikely to occur but because we lack a theoretical model to describe them. This issue is the subject of ongoing research as it has important practical applications in engineering. It is known from experiments in structural dynamics that the energy is very much likely to propagate along the junctions and stiffened elements. Thus the derivation of a transport theory for such guided waves is needed.

4. High-frequency power flow reflection/transmission coefficients in beam and plate assemblies

In this section, power flow reflection/transmission coefficients, also called efficiencies in the literature, of wave components in two coupled, semi-infinite beams or plates are computed. This issue is everything but new, and similar results have been reported recently by Ouisse and Guyader (2003) for Euler-Bernoulli beams and Kirchhoff-Love plates, or Norris (1998) for thick shells, among many other examples. However these studies are dedicated to the low-frequency range. In the high-frequency range, the energy wave components have a particular structure as shown in

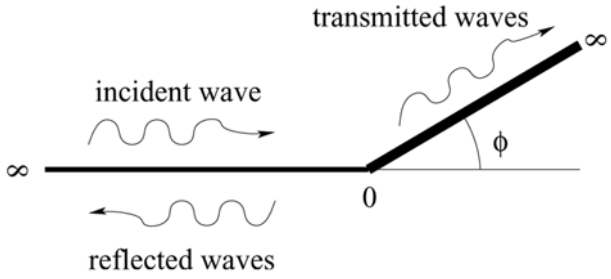

Fig. 2 Two coupled Timoshenko beams

section 2, and an adapted analysis has to be developped. It is detailed here for Timoshenko beams and then Mindlin plates.

4.1 Reflection/ transmission coefficients for coupled thick beams

Let us consider two semi-infinite thick beams (Timoshenko kinematics) defined by their curvilinear abscissa x such that $x \in \mathbb{R}_-$ for beam #1 and $x \in \mathbb{R}^+$ for beam #2. ϕ is the angle of the junction, see Fig. (2). The beams masses per unit length are ϱ_j for either $j = 1$ or $j = 2$, E_j are the Young's modulii, $G'_j = \kappa_j G_j$ are the reduced shear modulii where $\kappa_j < 1$ are the usual shear reduction factors, ν_j are the Poisson's coefficients, and $r_j = \sqrt{I_j / S_j}$ are the radii of gyration where I_j and S_j are respectively the cross-section inertias and areas. The equations of motion for both beams are given by Eq. (13), and the constitutive equations for their shear forces, bending moments and longitudinal forces are given by Eq. (12) (with $R = \infty$ for straight beams). Depending on the cutoff frequency $\omega_c = c_T / r$, the associated wavenumbers for plane waves propagating in beam #1 or beam #2 at the frequency ω are (dropping subscript j for clarity purposes):

$$k_a(\omega) = \sqrt{\frac{\omega^2}{2}\left(\frac{1}{c_P^2}+\frac{1}{c_T^2}\right) + \sqrt{\frac{\omega^2}{r^2 c_P^2} + \frac{\omega^4}{4}\left(\frac{1}{c_P^2}-\frac{1}{c_T^2}\right)^2}}$$

and:

$$\begin{cases} k_b(\omega) = \sqrt{\dfrac{\omega^2}{2}\left(\dfrac{1}{c_P^2}+\dfrac{1}{c_T^2}\right) - \sqrt{\dfrac{\omega^2}{r^2 c_P^2} + \dfrac{\omega^4}{4}\left(\dfrac{1}{c_P^2}-\dfrac{1}{c_T^2}\right)^2}} & \text{if } \omega > \omega_c \\ k_b(\omega) = i\sqrt{\sqrt{\dfrac{\omega^2}{r^2 c_P^2} + \dfrac{\omega^4}{4}\left(\dfrac{1}{c_P^2}-\dfrac{1}{c_T^2}\right)^2} - \dfrac{\omega^2}{2}\left(\dfrac{1}{c_P^2}+\dfrac{1}{c_T^2}\right)} & \text{if } \omega < \omega_c \end{cases}$$

for bending motions. They are $k_P(\omega) = \omega / c_P$ for longitudinal (compressional) motions, and $k_T(\omega) = \omega / c_T$ for a pure transverse shear motion. In the high-frequency range, both bending wavenumbers k_a and k_b are real. They may be written:

$$k_{\mathrm{a,\,b}}(\omega) = \frac{k_{\mathrm{T}}}{\sqrt{2}}\sqrt{1+\frac{c_{\mathrm{T}}^2}{c_{\mathrm{P}}^2} \pm \sqrt{4\frac{k_{\mathrm{E}}^4}{k_{\mathrm{T}}^4}+\left(1-\frac{c_{\mathrm{T}}^2}{c_{\mathrm{P}}^2}\right)^2}}$$

$$= \frac{k_{\mathrm{P}}}{\sqrt{2}}\sqrt{1+\frac{c_{\mathrm{P}}^2}{c_{\mathrm{T}}^2} \mp \sqrt{4\frac{k_{\mathrm{E}}^4}{k_{\mathrm{P}}^4}+\left(1-\frac{c_{\mathrm{P}}^2}{c_{\mathrm{T}}^2}\right)^2}}$$

where $k_{\mathrm{E}}(\omega) = \sqrt{\omega}\sqrt[4]{\frac{\varrho}{EI}}$ is the bending wavenumber of an Euler-Bernoulli (thin) beam, such that in the high-frequency limit $\mu = k_{\mathrm{E}} / k_{\mathrm{P}} \to 0$ we have $k_{\mathrm{a}} = k_{\mathrm{T}}$ and $k_{\mathrm{b}} = k_{\mathrm{P}}$. This remark and the results of section 2.3 suggest the following wave decomposition at higher frequencies, which is also compatible with Eq. (16).

An incident wave traveling in beam #1 in the direction of increasing x may be written either $w_i(x) = e^{-\mathrm{i}k_{\mathrm{T}1}x}$ for a pure shear motion, or $\theta_i(x) = -\mathrm{i}k_{\mathrm{P}1}e^{-\mathrm{i}k_{\mathrm{P}1}x}$ for a pure bending motion, or $u_i(x) = e^{-\mathrm{i}k_{\mathrm{P}1}x}$ for a longitudinal motion. Then the reflected waves are written:

$$w_r(x) = Ae^{\mathrm{i}k_{\mathrm{T}1}x},\ \theta_r(x) = \mathrm{i}k_{\mathrm{P}1}Be^{\mathrm{i}k_{\mathrm{P}1}x},\ u_r(x) = Fe^{\mathrm{i}k_{\mathrm{P}1}x}$$

and the transmitted waves are written:

$$w_t(x) = Ce^{-\mathrm{i}k_{\mathrm{T}2}x},\ \theta_t(x) = -\mathrm{i}k_{\mathrm{P}2}De^{-\mathrm{i}k_{\mathrm{P}2}x},\ u_t(x) = He^{-\mathrm{i}k_{\mathrm{P}2}x}$$

Coefficients A, B, C, D, F, and H are obtained from the continuity conditions of the displacements, rotations, forces and moments at the junction $x = 0$. They yield the linear system $[T]\mathbf{C} = [U]$ for $\mathbf{C} = (A, C, F, H)^{\mathrm{T}}$, with:

$$[T] = \begin{bmatrix} \cos\phi & -1 & \sin\phi & 0 \\ -\sin\phi & 0 & \cos\phi & -1 \\ \cos\phi & \frac{\varrho_2 c_{\mathrm{T}2}}{\varrho_1 c_{\mathrm{T}1}} & \frac{c_{\mathrm{P}1}}{c_{\mathrm{T}1}}\sin\phi & 0 \\ \sin\phi & 0 & -\frac{c_{\mathrm{P}1}}{c_{\mathrm{T}1}}\cos\phi & -\frac{\varrho_2 c_{\mathrm{P}2}}{\varrho_1 c_{\mathrm{T}1}} \end{bmatrix} \tag{37}$$

and:

$$[U] = \begin{bmatrix} -\cos\phi & 0 & -\sin\phi \\ \sin\phi & 0 & -\cos\phi \\ \cos\phi & \frac{c_{\mathrm{T}1}}{c_{\mathrm{P}2}}D\left(\frac{\varrho_2 c_{\mathrm{T}2}^2}{\varrho_1 c_{\mathrm{T}1}^2} - \cos\phi\right) & \frac{c_{\mathrm{P}1}}{c_{\mathrm{T}1}}\sin\phi \\ \sin\phi & -\frac{c_{\mathrm{T}1}}{c_{\mathrm{P}2}}D\sin\phi & -\frac{c_{\mathrm{P}1}}{c_{\mathrm{T}1}}\cos\phi \end{bmatrix} \tag{38}$$

for the incident waves; the first column of $[U]$ corresponds to a shear incident wave, the second one to a bending incident wave, and the third one to a longitudinal incident wave. Coefficients B and D are null for shear or longitudinal incident waves, and:

$$D^{-1} = \frac{1}{2}\left(\frac{c_{\mathrm{P}1}}{c_{\mathrm{P}2}}\right)\left(1+\frac{E_2 I_2 c_{\mathrm{P}1}}{E_1 I_1 c_{\mathrm{P}2}}\right), \quad B = 1 - \frac{c_{\mathrm{P}1}}{c_{\mathrm{P}2}} D \tag{39}$$

for a bending incident wave. The associated power flows are derived from the generic formula of the energy flux of plane waves propagating in a beam. The transient power flow is:

$$\Pi = -\Re\mathrm{e}\{N\overline{\partial_t u} + T\overline{\partial_t w} + M\overline{\partial_t \theta}\}$$

and then the time averaged power flow associated to traveling plane waves is:

$$\langle \Pi \rangle = \frac{1}{2}\Re\mathrm{e}\{\mathrm{i}\omega(N\bar{u} + T\bar{w} + M\bar{\theta})\}$$

The incident powers at the junction $x = 0$ are:

$$\langle \Pi_i^{\mathrm{T}} \rangle = \frac{1}{2}\omega G_1' S_1 k_{\mathrm{T}1}, \quad \langle \Pi_i^{\mathrm{b}} \rangle = \frac{1}{2}\omega E_1 I_1 k_{\mathrm{P}1}^3, \quad \langle \Pi_i^{\mathrm{n}} \rangle = \frac{1}{2}\omega E_1 S_1 k_{\mathrm{P}1}$$

for the shear, bending and longitudinal components, respectively. The reflected power flows at the junction are:

$$\langle \Pi_r^{\mathrm{T}} \rangle = -\frac{1}{2}\omega G_1' S_1 (k_{\mathrm{T}1}|A|^2 - k_{\mathrm{P}1}\Re\mathrm{e}\{\bar{A}B\})$$

for the shear component, and:

$$\langle \Pi_r^{\mathrm{b}} \rangle = -\frac{1}{2}\omega E_1 I_1 k_{\mathrm{P}1}^3 |B|^2, \quad \langle \Pi_r^{\mathrm{n}} \rangle = -\frac{1}{2}\omega E_1 S_1 k_{\mathrm{P}1}|F|^2$$

for the bending and longitudinal components, respectively. Here the minus sign indicates a reversed traveling direction. The transmitted power flows at the junction are:

$$\langle \Pi_t^{\mathrm{T}} \rangle = \frac{1}{2}\omega G_2' S_2 (k_{\mathrm{T}2}|C|^2 - k_{\mathrm{P}2}\Re\mathrm{e}\{\bar{C}D\})$$

for the shear component, and:

$$\langle \Pi_t^{\mathrm{b}} \rangle = \frac{1}{2}\omega E_2 I_2 k_{\mathrm{P}2}^3 |D|^2, \quad \langle \Pi_t^{\mathrm{n}} \rangle = \frac{1}{2}\omega E_2 S_2 k_{\mathrm{P}2}|H|^2$$

for the bending and longitudinal components, respectively.

These results are used to compute the various high-frequency power reflection/transmission coefficients for coupled Timoshenko beams by:

$$\rho_{\alpha\beta} = \frac{\langle \Pi_r^{\alpha} \rangle}{\langle \Pi_i^{\beta} \rangle}, \quad \tau_{\alpha\beta} = \frac{\langle \Pi_t^{\alpha} \rangle}{\langle \Pi_i^{\beta} \rangle}, \quad \alpha, \beta \in \{\mathrm{T}, \mathrm{b}, \mathrm{n}\} \tag{40}$$

They are independent of the frequency and are plotted as functions of the junction angle ϕ in the range $[0, \pi[$ on Fig. (3) and Fig. (4). Fig. (3) is for two identical beams: $E_1 = E_2$, $I_1 = I_2$, $\varrho_1 = \varrho_2$,

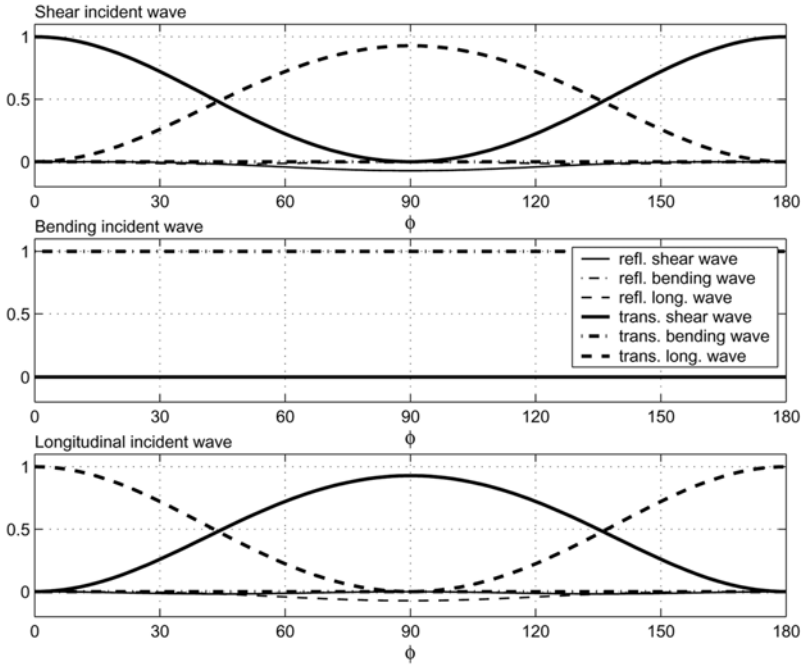

Fig. 3 High-frequency power flow reflection/transmission coefficients for two connected, semi-infinite Timoshenko beams; $E_1 = E_2$, $I_1 = I_2$, $\varrho_1 = \varrho_2$, and $\nu_1 = \nu_2 = 0.3$.

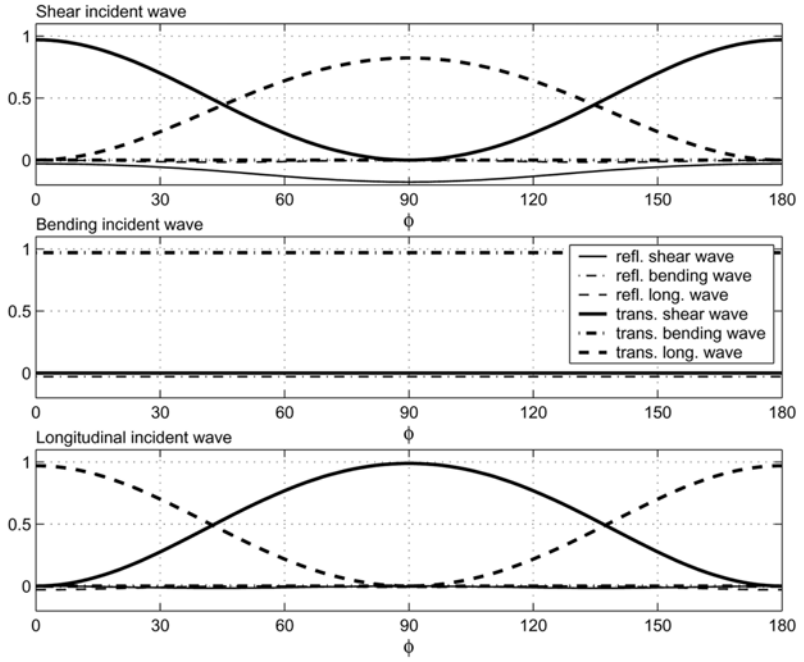

Fig. 4 High-frequency power flow reflection/transmission coefficients for two connected, semi-infinite Timoshenko beams; $2E_1 = E_2$, $I_1 = I_2$, $\varrho_1 = \varrho_2$, and $\nu_1 = \nu_2 = 0.3$.

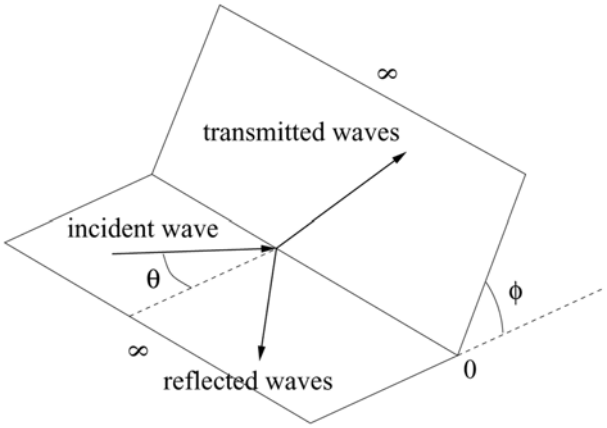

Fig. 5 Two coupled Mindlin plates

and $\nu_1 = \nu_2 = 0.3$, and Fig. (4) is for two different beams: $2E_1 = E_2$, all other parameters being unchanged. The high-frequency power flow reflection coefficients of a semi-infinite beam for either Dirichlet ($E_1 / E_2 \to 0$) or Neumann ($E_2 / E_2 \to 0$) boundary conditions at its end are directly obtained from these results. Computations show that they are all equal to 1 without mode conversion of any type.

4.2 Reflection/transmission coefficients for coupled thick plates

Let us now consider two semi-infinite thick plates (Mindlin kinematics) defined by their local coordinates (x, y) on the mid-surfaces, such that $x \in \mathbb{R}_-$ for plate #1 and $x \in \mathbb{R}_+$ for plate #2. The junction Γ is the line $\{x = 0\}$ and ϕ stands for the angle between the plates, see Fig. (5). Their masses per unit surface are ϱ_j for either $j = 1$ or $j = 2$, E_j are the Young's modulii, $G'_j = \kappa_j G_j$ are the reduced shear modulii where κ_j are the usual shear reduction factors, ν_j are the Poisson's coefficients, $G_j = \dfrac{E_j}{2(1+\nu_j)}$, and h_j are the thicknesses. The equations of motion for both plates are given Eq. (22), and the constitutive equations for their shear forces, bending moments and longitudinal forces are given by Eq. (21), with $\mathbb{B} = \mathbf{0}$ for flat plates. Depending on the cutoff frequency $\omega_c = \sqrt{12}\, c_T / k$, the associated wavenumbers for plane waves propagating in plate #1 or plate #2 at the frequency ω are (dropping subscript j for clarity purposes) $k_P(\omega) = \dfrac{\omega}{c_P}$, $k_S(\omega) = \dfrac{\omega}{c_S}$ for the in-plane motions, and:

$$k_a(\omega) = \sqrt{\frac{1}{2}(k_P^2 + k_T^2) + \sqrt{k_E^4 + \frac{1}{4}(k_T^2 - k_P^2)^2}}$$

$$k_b(\omega) = \sqrt{\frac{1}{2}(k_P^2 + k_T^2) - \sqrt{k_E^4 + \frac{1}{4}(k_T^2 - k_P^2)^2}} \quad \text{if } \omega \geq \omega_c$$

$$k_b(\omega) = \mathrm{i}\sqrt{\sqrt{k_E^4 + \frac{1}{4}(k_T^2 - k_P^2)^2} - \frac{1}{2}(k_P^2 + k_T^2)} \quad \text{if } \omega < \omega_c$$

$$k_c(\omega) = \frac{k_a k_b k_S}{k_P k_T}$$

for the bending motion, introducing $k_T(\omega) = \frac{\omega}{c_T}$ and $k_E(\omega) = \sqrt{\omega}\sqrt[4]{\frac{\varrho}{D}}$ for the bending wavenumber of a thin plate (Kirchhoff-Love kinematics such that $\boldsymbol{\theta} = -\nabla_\Sigma w$). Observe that if k_b is purely imaginary, so is k_c. In the high-frequency limit $\mu = \frac{k_E}{k_P} \to 0$ we have $k_a = k_T$, $k_b = k_P$, and $k_c = k_S$.

The analysis in section 2.4 has shown that five propagating modes exist in this limit: two modes with wavenumber k_P, two modes with wavenumber k_S, and one mode with wavenumber k_T. These wavenumbers are now written $k_P^2 = \chi_P^2 + k^2$, $k_S^2 = \chi_S^2 + k^2$, and $k_T^2 = \chi_T^2 + k^2$, where $k \in \mathbb{R}$ is the tangent (parallel to the junction) wavenumber which is kept unchanged by the reflection/transmission processes owing to Snell-Descartes law. It is always a real number for propagating waves. However χ_P, χ_S, and χ_T may be either real for propagating, far-field waves, or purely imaginary for evanescent, near-field waves, depending on the value of k with respect to k_P, k_S, and k_T, respectively. These remarks and the results of section 2.4 suggest the following wave decomposition at higher frequencies, which is also compatible with Eq. (25).

Incident waves traveling in plate #1 in the direction of increasing x with an angle θ with respect to the normal to the junction may be written either:

$$w_i(x,y) = e^{-\mathrm{i}k_{T1}(x\cos\theta + y\sin\theta)}, \quad k = k_{T1}\sin\theta$$

for quasi-shear motion, or:

$$\boldsymbol{\theta}_{Pi}(x,y) = -\mathrm{i}k_{P1}\begin{pmatrix}\cos\theta\\ \sin\theta\end{pmatrix} e^{-\mathrm{i}k_{P1}(x\cos\theta + y\sin\theta)}, k = k_{P1}\sin\theta$$

$$\boldsymbol{\theta}_{Si}(x,y) = -\mathrm{i}k_{S1}\begin{pmatrix}-\sin\theta\\ \cos\theta\end{pmatrix} e^{-\mathrm{i}k_{S1}(x\cos\theta + y\sin\theta)}, k = k_{S1}\sin\theta$$

for quasi-bending motions, or:

$$\mathbf{u}_{Pi}(x,y) = \begin{pmatrix}\cos\theta\\ \sin\theta\end{pmatrix} e^{-\mathrm{i}k_{P1}(x\cos\theta + y\sin\theta)}, k = k_{P1}\sin\theta$$

$$\mathbf{u}_{Si}(x,y) = \begin{pmatrix}-\sin\theta\\ \cos\theta\end{pmatrix} e^{-\mathrm{i}k_{S1}(x\cos\theta + y\sin\theta)}, k = k_{S1}\sin\theta$$

for in-plane motions. The transmitted waves in plate #1 may be written:

$$w_r(x,y) = Ae^{\mathrm{i}(\chi_{T1}x - ky)}$$

for quasi-shear motion,

$$\boldsymbol{\theta}_r(x,y) = \mathrm{i}B\begin{pmatrix}-\chi_{P1}\\ k\end{pmatrix} e^{\mathrm{i}(\chi_{P1}x - ky)} + \mathrm{i}F\begin{pmatrix}k\\ \chi_{S1}\end{pmatrix} e^{\mathrm{i}(\chi_{S1}x - ky)}$$

for quasi-bending motions, and:

$$\mathbf{u}_r(x,y) = \frac{H}{k_{\mathrm{P1}}}\begin{pmatrix}-\chi_{\mathrm{P1}}\\ k\end{pmatrix}e^{\mathrm{i}(\chi_{\mathrm{P1}}x-ky)} + \frac{I}{k_{\mathrm{S1}}}\begin{pmatrix}k\\ \chi_{\mathrm{S1}}\end{pmatrix}e^{\mathrm{i}(\chi_{\mathrm{S1}}x-ky)}$$

for in-plane motions. The transmitted waves in plate #2 may be written:

$$w_t(x,y) = Je^{\mathrm{i}(\chi_{\mathrm{T2}}x+ky)}$$

for quasi-shear motion,

$$\theta_t(x,y) = -\mathrm{i}K\begin{pmatrix}\chi_{\mathrm{P2}}\\ k\end{pmatrix}e^{-\mathrm{i}(\chi_{\mathrm{P2}}x+ky)} - iL\begin{pmatrix}-k\\ \chi_{\mathrm{S2}}\end{pmatrix}e^{-\mathrm{i}(\chi_{\mathrm{S2}}x+ky)}$$

for quasi-bending motions, and:

$$\mathbf{u}_t(x,y) = \frac{M}{k_{\mathrm{P2}}}\begin{pmatrix}\chi_{\mathrm{P2}}\\ k\end{pmatrix}e^{-\mathrm{i}(\chi_{\mathrm{P2}}x+ky)} + \frac{N}{k_{\mathrm{S2}}}\begin{pmatrix}-k\\ \chi_{\mathrm{S2}}\end{pmatrix}e^{-\mathrm{i}(\chi_{\mathrm{S2}}x+ky)}$$

for in-plane motions. Coefficients A, B, F, H, I, J, K, L, M and N are obtained from the continuity conditions at the junction $x = 0$, that is, if $\hat{\mathbf{n}}$ is the unit normal to Γ, $\{\mathbf{u}_\Sigma, \theta, w\}$ and $\{\mathbb{N}\hat{\mathbf{n}}, \mathbb{M}\hat{\mathbf{n}}, \mathbf{T}\cdot\hat{\mathbf{n}}\}$ are continuous across the junction. These conditions yield two linear systems: $[\mathcal{S}]\mathbf{C} = [U]$ for $\mathbf{C} = (B, F, K, L)$, with:

$$[S] = \begin{bmatrix} \frac{\chi_{\mathrm{P1}}}{k_{\mathrm{P1}}} & -\frac{k}{k_{\mathrm{P1}}} & -\frac{\chi_{\mathrm{P2}}}{k_{\mathrm{P1}}} & \frac{k}{k_{\mathrm{P1}}} \\ \frac{k}{k_{\mathrm{S1}}} & \frac{\chi_{\mathrm{S1}}}{k_{\mathrm{S1}}} & \frac{k}{k_{\mathrm{S1}}} & \frac{\chi_{\mathrm{S2}}}{k_{\mathrm{S1}}} \\ \frac{\chi_{\mathrm{P1}}^2+\nu_1 k^2}{k_{\mathrm{P1}}^2} & -2\frac{\chi_{\mathrm{S1}}k}{k_{\mathrm{S1}}^2} & \frac{\varrho_2 h_2^2}{\varrho_1 h_1^2}\left(\frac{\chi_{\mathrm{P2}}^2+\nu_2 k^2}{k_{\mathrm{P2}}^2}\right) & -2\frac{\varrho_2 h_2^2}{\varrho_1 h_1^2}\left(\frac{\chi_{\mathrm{S2}}k}{k_{\mathrm{S2}}^2}\right) \\ 2\frac{\chi_{\mathrm{P1}}k}{k_{\mathrm{S1}}^2} & \frac{\chi_{\mathrm{S1}}^2-k^2}{k_{\mathrm{S1}}^2} & -2\frac{\varrho_2 h_2^2}{\varrho_1 h_1^2}\left(\frac{\chi_{\mathrm{P2}}k}{k_{\mathrm{S2}}^2}\right) & \frac{\varrho_2 h_2^2}{\varrho_1 h_1^2}\left(\frac{k^2-\chi_{\mathrm{S2}}^2}{k_{\mathrm{S2}}^2}\right) \end{bmatrix} \tag{41}$$

and:

$$[U] = \begin{bmatrix} -\cos\theta & \frac{k_{\mathrm{S1}}}{k_{\mathrm{P1}}}\sin\theta \\ \frac{k_{\mathrm{P1}}}{k_{\mathrm{S1}}}\sin\theta & \cos\theta \\ \cos^2\theta+\nu_1\sin^2\theta & -\sin 2\theta \\ -\frac{k_{\mathrm{P1}}^2}{k_{\mathrm{S1}}^2}\sin 2\theta & -\cos 2\theta \end{bmatrix} \tag{42}$$

and $[T]\,\mathbf{D} = [V]$ for $\mathbf{D} = (A, H, I, J, M, N)$, with:

$$[T] = \begin{bmatrix} -1 & 0 & 0 & \cos\phi & \frac{\chi_{P2}}{k_{P2}}\sin\phi & -\frac{k}{k_{S2}}\sin\phi \\ 0 & \frac{\chi_{P1}}{k_{P1}} & -\frac{k}{k_{S1}} & -\sin\phi & \frac{\chi_{P2}}{k_{P2}}\cos\phi & -\frac{k}{k_{S2}}\cos\phi \\ 0 & -\frac{k}{k_{P1}} & -\frac{\chi_{S1}}{k_{S1}} & 0 & \frac{k}{k_{P2}} & \frac{\chi_{S2}}{k_{S2}} \\ \frac{\chi_{T1}}{k_{T1}} & 0 & 0 & \frac{\varrho_2 c_{T2}}{\varrho_1 c_{T1}}\left(\frac{\chi_{T2}}{k_{T2}}\right)\cos\phi & \frac{\varrho_2 c_{P2}}{\varrho_1 c_{T1}}\left(\frac{\chi_{P2}^2+\nu_2 k^2}{k_{P2}^2}\right)\sin\phi & -2\frac{\varrho_2 c_{S2}}{\varrho_1 c_{T1}}\left(\frac{\chi_{S2}k}{k_{S2}^2}\right)\sin\phi \\ 0 & -\left(\frac{\chi_{P1}^2+\nu_1 k^2}{k_{P1}^2}\right) & 2\frac{c_{S1}}{c_{P1}}\left(\frac{\chi_{S1}k}{k_{S1}^2}\right) & -\frac{\varrho_2 c_{T2}}{\varrho_1 c_{T1}}\left(\frac{\chi_{T2}}{k_{T2}}\right)\sin\phi & \frac{\varrho_2 c_{P2}}{\varrho_1 c_{T1}}\left(\frac{\chi_{P2}^2+\nu_2 k^2}{k_{P2}^2}\right)\cos\phi & -2\frac{\varrho_2 c_{S2}}{\varrho_1 c_{T1}}\left(\frac{\chi_{S2}k}{k_{S2}^2}\right)\cos\phi \\ 0 & 2\frac{\chi_{P1}k}{k_{P1}k_{S1}} & \frac{\chi_{S1}^2-k^2}{k_{S1}^2} & 0 & 2\frac{\varrho_2 c_{S2}}{\varrho_1 c_{S1}}\left(\frac{\chi_{P2}k}{k_{P2}k_{S2}}\right) & \frac{\varrho_2 c_{S2}}{\varrho_1 c_{S1}}\left(\frac{\chi_{S2}^2-k^2}{k_{S2}^2}\right) \end{bmatrix} \tag{43}$$

$$[V] = \begin{bmatrix} 1 & 0 & 0 & 0 & 0 \\ 0 & 0 & 0 & \cos\theta & -\sin\theta \\ 0 & 0 & 0 & \sin\theta & \cos\theta \\ \cos\theta f_1(\phi) & -\frac{k_{P1}}{k_{T1}}\cos\theta & f_1(\phi)+\frac{k_{S1}}{k_{T1}}\sin\theta & 0 & 0 \\ 0 & f_2(\phi) & f_2(\phi) & \cos^2\theta+\nu_1\sin^2\theta & -\frac{k_{P1}}{k_{S1}}\sin 2\theta \\ 0 & 0 & 0 & \frac{k_{P1}}{k_{S1}}\sin 2\theta & \cos 2\theta \end{bmatrix} \tag{44}$$

f_1 and f_2 depend on the solution $\mathbf{C}$ of the previous system by:

$$f_1(\phi) = -\frac{\chi_{P1}}{k_{T1}}B + \frac{k}{k_{T1}}F + \frac{\varrho_2 k_{T1}}{\varrho_1 k_{T2}}\left(\frac{\chi_{P2}}{k_{T2}}K - \frac{k}{k_{T2}}L\right)\cos\phi$$

$$f_2(\phi) = -\frac{\varrho_2 k_{P1}}{\varrho_1 k_{T2}}\left(\frac{\chi_{P2}}{k_{T2}}K - \frac{k}{k_{T2}}L\right)\sin\phi$$

The columns of $[U]$ correspond to quasi-bending incident waves. The first column of $[V]$ corresponds to a quasi-shear incident wave, the second and third ones correspond to quasi-bending incident waves, and the fourth and fifth ones correspond to in-plane incident waves. The associated power flows are derived from the generic formula of the energy flux of plane waves propagating in a plate. The transient power flow is:

$$\Pi = -\Re\mathrm{e}\{\mathbb{N}\bar{\dot{\mathbf{u}}} + \mathbb{M}\bar{\dot{\boldsymbol{\theta}}} + \mathbf{T}\bar{\dot{w}}\}$$

and then the time averaged power flow associated to traveling plane waves is:

$$\langle \boldsymbol{\Pi} \rangle = \frac{1}{2}\Re\mathrm{e}\{\mathrm{i}\omega(\mathbb{N}\bar{\mathbf{u}} + \mathbb{M}\bar{\boldsymbol{\theta}} + \mathbf{T}\bar{w})\}$$

The incident power at the junction $x = 0$ is thus:

$$\langle \Pi_i^{\mathrm{T}} \rangle = \frac{1}{2}\omega^2 \varrho_1 c_{\mathrm{T}1} \begin{pmatrix} \cos\theta \\ \sin\theta \end{pmatrix}$$

for the quasi-shear component,

$$\langle \Pi_i^{\mathrm{Pb}} \rangle = \frac{1}{2}\omega^2 \varrho_1 c_{\mathrm{P}1} \frac{k_{\mathrm{P}1}^4}{k_{\mathrm{E}1}^4} \begin{pmatrix} \cos\theta \\ \sin\theta \end{pmatrix}, \quad \langle \Pi_i^{\mathrm{Sb}} \rangle = \frac{1}{2}\omega^2 \varrho_1 c_{\mathrm{S}1} \frac{k_{\mathrm{P}1}^2 k_{\mathrm{S}1}^2}{k_{\mathrm{E}1}^4} \begin{pmatrix} \cos\theta \\ \sin\theta \end{pmatrix}$$

for the quasi-bending components, and:

$$\langle \Pi_i^{\mathrm{Pn}} \rangle = \frac{1}{2}\omega^2 \varrho_1 c_{\mathrm{P}1} \begin{pmatrix} \cos\theta \\ \sin\theta \end{pmatrix}, \quad \langle \Pi_i^{\mathrm{Sn}} \rangle = \frac{1}{2}\omega^2 \varrho_1 c_{\mathrm{S}1} \begin{pmatrix} \cos\theta \\ \sin\theta \end{pmatrix}$$

for the in-plane components. The reflected power flows away from the junction are:

$$\langle \Pi_r^{\mathrm{T}} \rangle = \frac{1}{2}\omega \varrho_1 c_{\mathrm{T}1}^2 \left[|A|^2 \begin{pmatrix} -\Re\mathrm{e}\{\chi_{\mathrm{T}1}\} \\ k \end{pmatrix} + AB \begin{pmatrix} -\Re\mathrm{e}\{\chi_{\mathrm{P}1}\} \\ k \end{pmatrix} + AF \begin{pmatrix} k \\ \Re\mathrm{e}\{\chi_{\mathrm{S}1}\} \end{pmatrix} \right]$$

for the quasi-shear component,

$$\langle \Pi_r^{\mathrm{b}} \rangle = \frac{1}{2}\omega \varrho_1 c_{\mathrm{T}1}^2 \frac{k_{\mathrm{P}1}^4}{k_{\mathrm{E}1}^4} \left[|B|^2 \begin{pmatrix} -\Re\mathrm{e}\{\chi_{\mathrm{P}1}\} \\ k \end{pmatrix} + |F|^2 \begin{pmatrix} -\Re\mathrm{e}\{\chi_{\mathrm{S}1}\} \\ k \end{pmatrix} \right]$$

for the quasi-bending components, and:

$$\langle \Pi_r^{\mathrm{n}} \rangle = \frac{1}{2}\omega \varrho_1 \left[c_{\mathrm{P}1}^2 |H|^2 \begin{pmatrix} -\Re\mathrm{e}\{\chi_{\mathrm{P}1}\} \\ k \end{pmatrix} + c_{\mathrm{S}1}^2 |I|^2 \begin{pmatrix} -\Re\mathrm{e}\{\chi_{\mathrm{S}1}\} \\ k \end{pmatrix} \right]$$

for the in-plane components. The transmitted power flows away from the junction are:

$$\langle \Pi_t^{\mathrm{T}} \rangle = \frac{1}{2}\omega \varrho_2 c_{\mathrm{T}2}^2 \left[|J|^2 \begin{pmatrix} \Re\mathrm{e}\{\chi_{\mathrm{T}2}\} \\ k \end{pmatrix} - JK \begin{pmatrix} \Re\mathrm{e}\{\chi_{\mathrm{P}2}\} \\ k \end{pmatrix} - JL \begin{pmatrix} -k \\ \Re\mathrm{e}\{\chi_{\mathrm{S}2}\} \end{pmatrix} \right]$$

for the quasi-shear component,

$$\langle \Pi_t^{\mathrm{b}} \rangle = \frac{1}{2}\omega \varrho_2 c_{\mathrm{P}2}^2 \frac{k_{\mathrm{P}2}^4}{k_{\mathrm{E}2}^4} \left[|K|^2 \begin{pmatrix} \Re\mathrm{e}\{\chi_{\mathrm{P}2}\} \\ k \end{pmatrix} + |L|^2 \begin{pmatrix} \Re\mathrm{e}\{\chi_{\mathrm{S}2}\} \\ k \end{pmatrix} \right]$$

for the quasi-bending components, and:

$$\langle \Pi_r^{\mathrm{n}} \rangle = \frac{1}{2}\omega \varrho_2 \left[c_{\mathrm{P}2}^2 |M|^2 \begin{pmatrix} \Re\mathrm{e}\{\chi_{\mathrm{P}2}\} \\ k \end{pmatrix} + c_{\mathrm{S}2}^2 |N|^2 \begin{pmatrix} \Re\mathrm{e}\{\chi_{\mathrm{S}2}\} \\ k \end{pmatrix} \right]$$

for the in-plane components.

These results are used to compute the various high-frequency power reflection/transmission

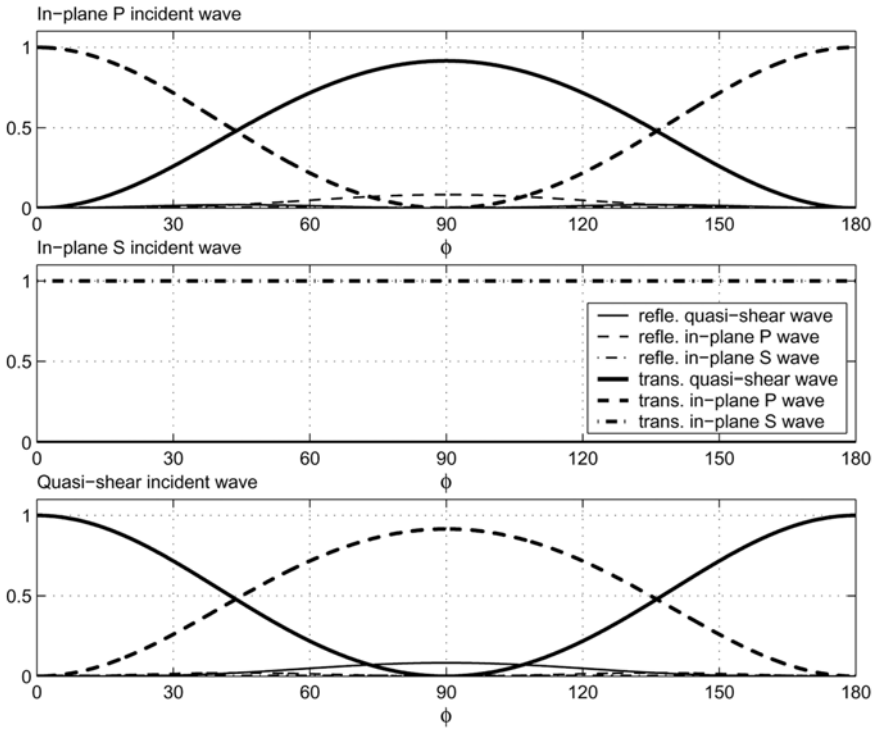

Fig. 6 High-frequency power flow reflection/transmission coefficients for two connected, semi-infinite Mindlin plates; incidence angle $\theta = 0^{\circ}$, $E_1 = E_2$, $h_1 = h_2$, $\varrho_1 = \varrho_2$, and $\nu_1 = \nu_2 = 0.3$.

coefficients for coupled Mindlin plates by:

$$\rho_{\alpha\beta}^{11} = -\frac{\langle \Pi_r^{\alpha} \cdot \hat{\mathbf{n}}_1 \rangle}{\langle \Pi_i^{\beta} \cdot \hat{\mathbf{n}}_1 \rangle}, \quad \tau_{\alpha\beta}^{12} = -\frac{\langle \Pi_t^{\alpha} \cdot \hat{\mathbf{n}}_2 \rangle}{\langle \Pi_i^{\beta} \cdot \hat{\mathbf{n}}_1 \rangle}, \quad \alpha, \beta \in \{\mathrm{T}, \mathrm{Pn}, \mathrm{Pb}, \mathrm{Sn}, \mathrm{Sb}\} \tag{45}$$

They are frequency-independent and plotted as functions of the junction angle $\phi \in [0, \pi[$ on Fig. (6) through Fig. (8) for various incidence angle θ and two identical plates: $E_1 = E_2$, $h_1 = h_2$, $\varrho_1 = \varrho_2$, and $\nu_1 = \nu_2 = 0.3$. The high-frequency power flow reflection coefficients of a semi-infinite thick plate for either Dirichlet or Neumann boundary conditions at its end are directly obtained from these results in the limit cases $E_1/E_2 \to 0$ (Dirichlet) and $E_2/E_1 \to 0$ (Neumann). The analysis yields the expected boundary reflection laws for a single plate with due consideration of the critical incidence angle:

$$\theta_c = \arcsin\sqrt{\frac{1-\nu}{2}}$$

and of course no transmission. The reflection coefficients as functions of the incidence angle θ are plotted on Fig. (9) and Fig. (10) for both conditions with $\nu = 0.3$, so that $\theta_c \simeq 36^{\circ}$. One can observe that the quasi-shear flow is uncoupled from the in-plane and quasi-bending flows in both cases, independently of the incidence direction. Mode conversions occur only for P and S components.

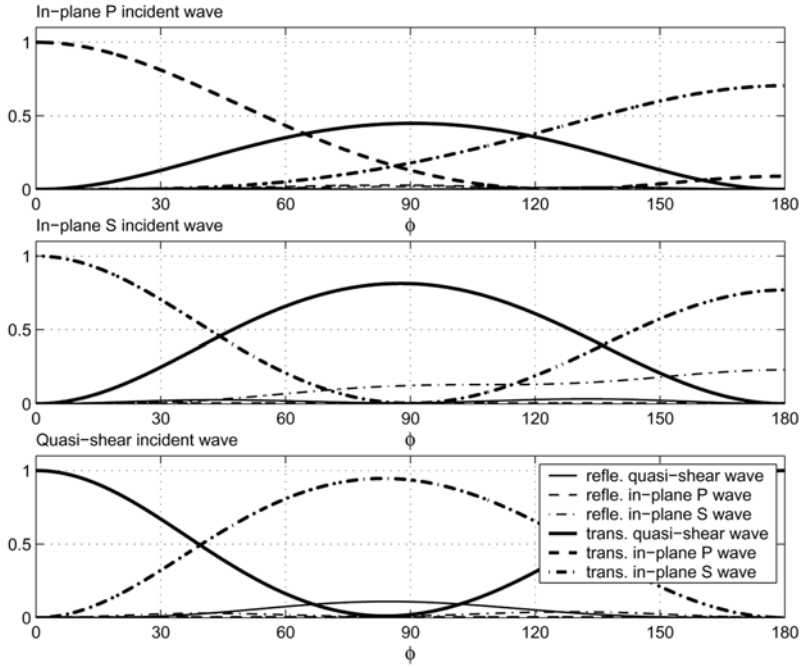

Fig. 7 High-frequency power flow reflection/transmission coefficients for two connected, semi-infinite Mindlin plates; incidence angle $\theta = 45^{o}$, $E_1 = E_2$, $h_1 = h_2$, $\varrho_1 = \varrho_2$, and $\nu_1 = \nu_2 = 0.3$.

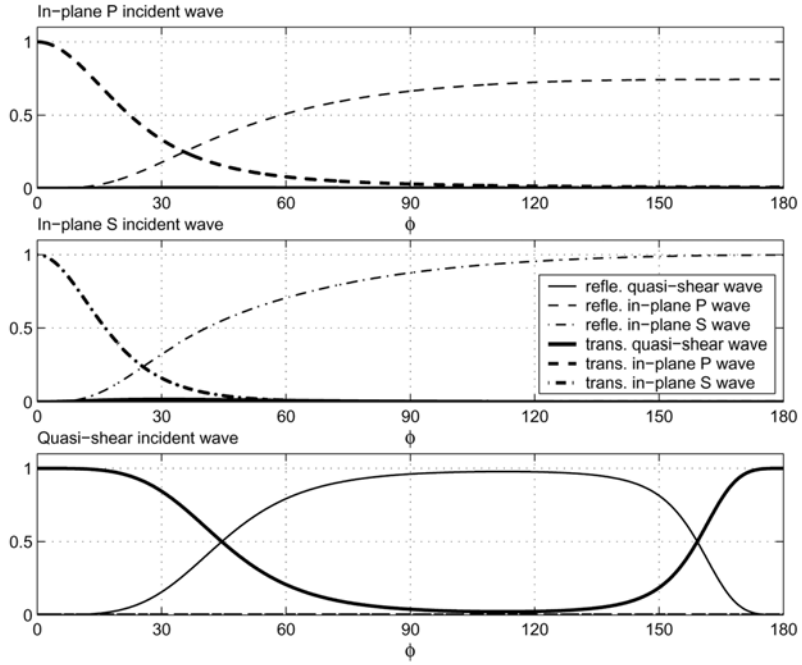

Fig. 8 High-frequency power flow reflection/transmission coefficients for two connected, semi-infinite Mindlin plates; incidence angle $\theta = 89^{o}$, $E_1 = E_2$, $h_1 = h_2$, $\varrho_1 = \varrho_2$, and $\nu_1 = \nu_2 = 0.3$.

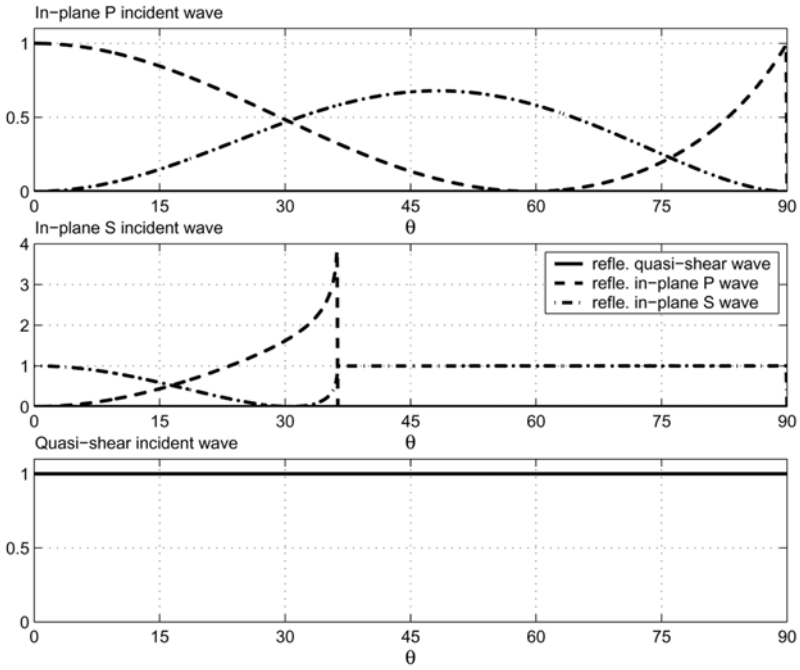

Fig. 9 High-frequency power flow reflection coefficients for a semi-infinite Mindlin plates with Dirichlet boundary condition; $\nu = 0.3$.

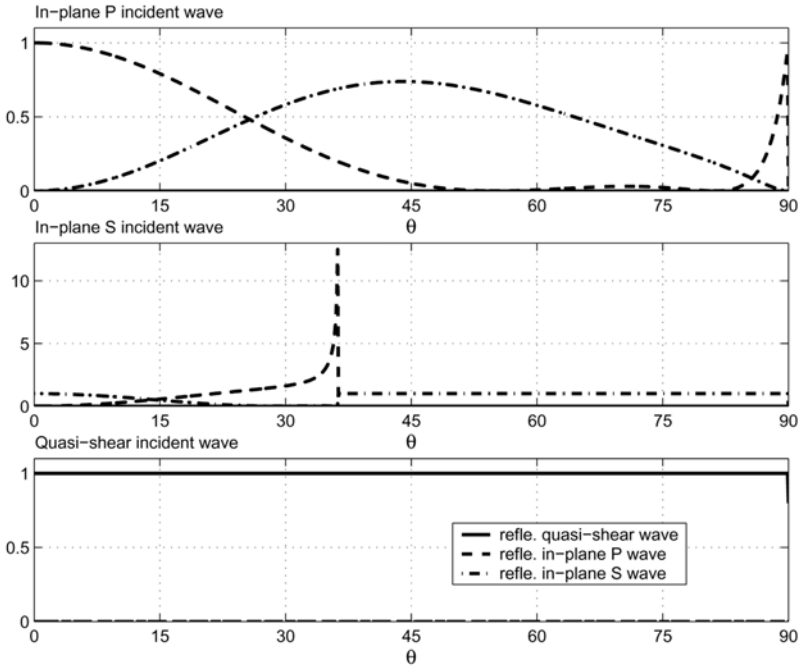

Fig. 10 High-frequency power flow reflection coefficients for a semi-infinite Mindlin plates with Neumann boundary condition; $\nu = 0.3$.

5. Numerical examples

In this section the transport equations (32) with the boundary conditions (34)-(35) and Hamiltonians $\lambda_\alpha^r = c_\alpha^r|\mathbf{k}|$ are solved numerically by either a finite element method or a direct Monte-Carlo method. Assemblies of two beams and two plates are considered, assuming that the materials are homogeneous such that $\nabla_\mathbf{x} c_\alpha^r = \mathbf{0}$ for both systems, $r = 1, 2$. Then the transport equations reduce to:

$$\partial_t \mathbf{W}_\alpha^r \pm c_\alpha^r \hat{\mathbf{k}} \cdot \nabla_\mathbf{x} \mathbf{W}_\alpha^r = \mathbf{0}$$

within each substructure. These equations have a trivial solution:

$$\mathbf{W}_\alpha^r(\mathbf{x}, \hat{\mathbf{k}}, t) = \mathbf{W}_\alpha^0(\mathbf{x} \mp c_\alpha^r \hat{\mathbf{k}} t), \quad r = 1, 2 \tag{46}$$

given the initial condition $\mathbf{W}_\alpha^r(\mathbf{x}, \hat{\mathbf{k}}, 0) = \mathbf{W}_\alpha^0(\mathbf{x})$, but ignoring the boundary/interface conditions. The latter induce scattering and mode conversions of the Wigner matrices $\mathbf{W}_\alpha^r$, which otherwise keep their initial wavefront shape as indicated by Eq. (46). The purpose of the numerical examples presented here is to illustrate this transport regime and the scattering effects of the interfaces and boundaries.

5.1 Coupled beams

We first consider a system of two coupled Timoshenko beams $]-L, 0[\cup]0, L$, $L > 0$, connected at $x = 0$ and such that beam #2 forms an angle $\phi = 60^\circ$ with beam #1. The transport equations (17) and (18) written for each beam are solved numerically by a finite element method, where the energy rays for the modes $\alpha = \mathrm{T}$ or P are reflected/transmitted by the junction at $x = 0$ or the free boundaries at $x = \pm L$ according to the scattering laws derived in section 4.1. The "Galerkin" discontinuous finite element method used here is described in (Savin (2005a, 2007)). In this method, the power flow reflection/transmission coefficients computed in section 4 are directly used to define the numerical fluxes at the junctions between two adjacent substructures or elements. The upward and downward flows are written as the superposition of reflected and transmitted flows including all existing energy modes. The formulation is otherwise standard.

The initial condition is a shear load applied to beam #1:

$$\mathrm{w}_\mathrm{T}^1(x, k, 0) = e^{-\ln 2\left(\frac{x - x_0}{r_0}\right)^2} \otimes \delta(k - k_0)$$

The overall system is partitioned into 200 uniform spatial elements. Legendre polynomials up to the second order are used as local basis functions, and Eqs. (17)-(18) are integrated in time by a fifth-order Runge-Kutta-Fehlberg scheme. The energy density of Eq. (19) is displayed on Fig. (11) and Fig. (12) for either $E_1 = E_2$ or $2E_1 = E_2$, respectively; all other parameters are equal, with $\nu_1 = \nu_2 = 0.3$. We choose $x_0 = -0.1 \times L$, $r_0 = 0.4 \times L$, and $\hat{k}_0 = +1$ for the initial condition. The time scale is $\tau = L / c_{\mathrm{T}2}$, the time needed by the wavefront to reach the extremity $x = L$ of beam #2 starting from the junction. The initial wavefront T is propagated from the left to the right ($k_0 > 0$) and reaches the junction at $t = 0.1 \times \tau$, where it is transmitted into two wavefronts T and P in beam #2 as seen on Fig. (11) or Fig. (12) at $t = 0.5 \times \tau$. The reflected wavefront T can also be seen on these plots, although for $E_1 = E_2$ its amplitude is relatively much lower than that of the transmitted

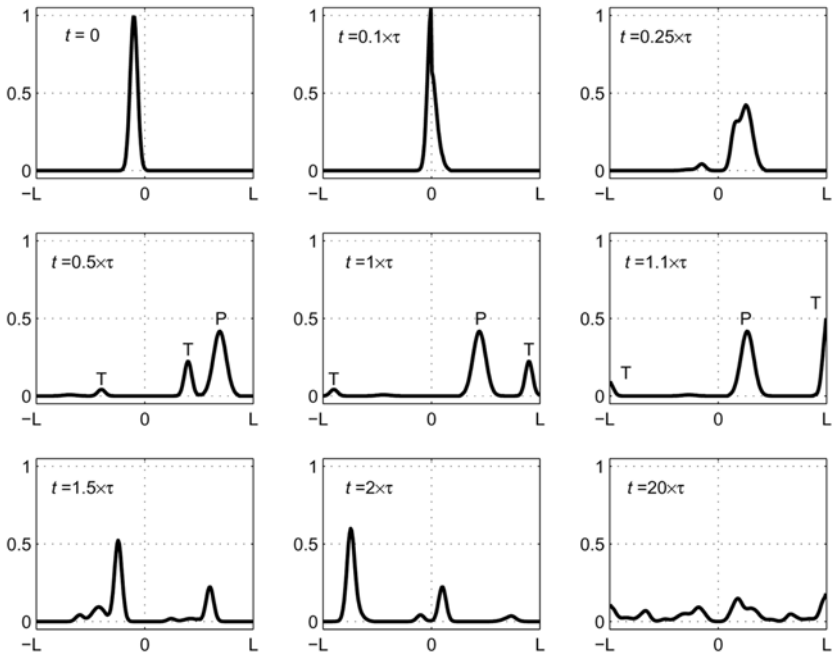

Fig. 11 Evolution of the energy density in a beam assembly impacted by a shear load with $\phi = 60^{o}$, $E_1 = E_2$, $I_1 = I_2$, $\varrho_1 = \varrho_2$, and $\nu_1 = \nu_2 = 0.3$.

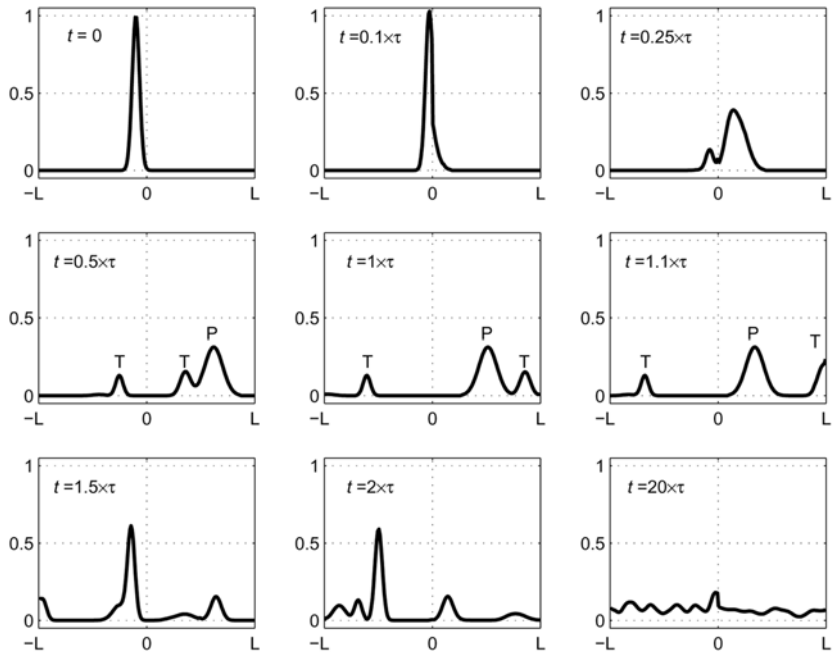

Fig. 12 Evolution of the energy density in a beam assembly impacted by a shear load with $\phi = 60^{o}$, $2E_1 = E_2$, $I_1 = I_2$, $\varrho_1 = \varrho_2$, and $\nu_1 = \nu_2 = 0.3$.

signals. The reflected wavefront P is almost indistinguishable, but it is not nil. At $t = 1.1 \times \tau$ the T wavefront reaches the extremity $x = L$ of the assembly and its amplitude here is twice the streaming amplitude because the forward and backward waves sum up; the P wavefront has already been reflected since $c_P > c_T$. The process of reflection and transmission at the junction and the free ends continues at later times, spreading gradually the wavefronts over the entire system; see Fig. (11) or Fig. (12) at $t = 20 \times \tau$. This smoothing of the energy levels corresponds to the emergence of a diffusive regime, as explained more in detail in the next example.

5.2 Coupled plates

An assembly of two homogeneous thick plates with $\phi = 60^o$ is now considered. Plate #1 is impacted at $t = 0$ by a mechanical shock at $\mathbf{x} = \mathbf{x}_0$ close to the junction line $\{x = 0\}$ which initially loads the shear mode T:

$$w_T^1(\mathbf{x}, \hat{\mathbf{k}}, 0) = \delta(\mathbf{x} - \mathbf{x}_0)$$

The transport equations (26) and (27) written for each plate are solved numerically by a direct Monte-Carlo method (see e.g. Lapeyre *et al.* (1998)), where the energy rays for the modes $\alpha = $ P, S or T are reflected/transmitted by the junction or the free boundaries (Neumann condition) according to the scattering laws derived in section 4.2. Both plates have identical parameters with $\nu_1 = \nu_2 = 0.3$. The evolution of the energy density of Eq. (29) is displayed on Fig. (13), where $\tau = \frac{L}{c_T}$, L is the

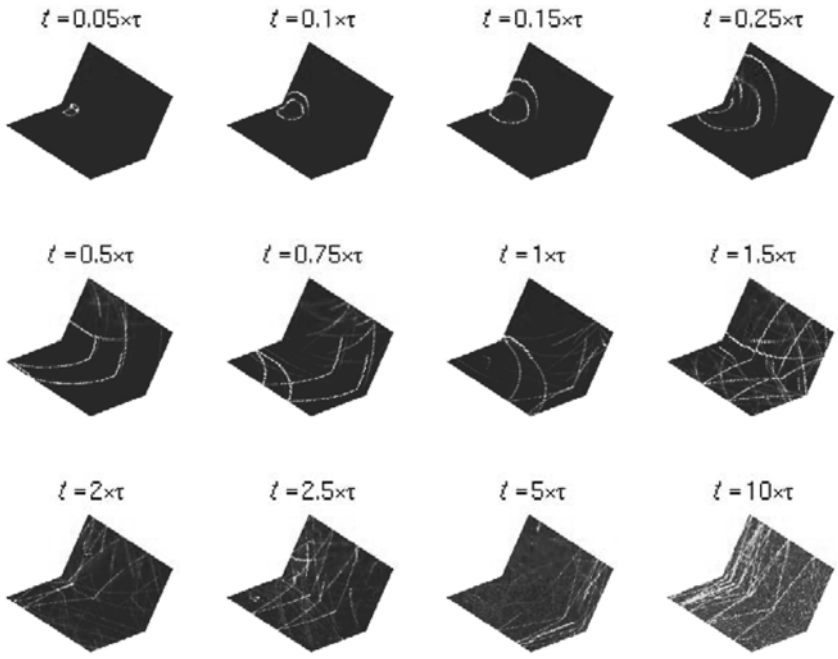

Fig. 13 Evolution of the energy density in a plate assembly impacted by a shear farce with $\phi = 60^o$, $E_1 = E_2$, $h_1 = h_2$, $\varrho_1 = \varrho_2$, and $\nu_1 = \nu_2 = 0.3$.

length of the plates and $L/2$ is their width. It can be observed that as soon as $t \simeq 10 \times \tau$ the phase information of the initial wavefront is almost lost, and a diffusive regime arises. In the diffusion limit the specific intensities become independent of the wavefront direction $\hat{\mathbf{k}}$. This regime, which is due here to the presence of the junction and the boundaries, may also arise in the presence of random heterogeneities of the medium at a length scale comparable with the (small) wavelength, as shown elsewhere; see for example Papanicolaou and Ryzhik (1999), Savin (2006). It is important to note at this stage that the presence of such singularities, namely interfaces, boundaries, or small random heterogeneities, is essential in the emergence of a diffusive regime in elastic and other media. The latter is obtained as the asymptotic limit of the transport regime described in section 2 at late times or for a short scattering mean free path, which is the mean distance traveled by a wave before it is scattered in some way. These fundamental and well-known results are in basic contradiction with the vibrational conductivity analogy of the structural acoustics literature (Nefske and Sung 1989), where a diffusive regime is assumed improperly for unbounded, homogeneous media, ignoring the necessary conditions recalled above for its emergence. If these conditions are not fulfilled, the scattering mean free path may be infinite and the transport regime is the sole regime holding for the high-frequency energy density.

6. Conclusions

In this paper a model of transport for the high-frequency vibrational energy density in a coupled system has been introduced. It is assumed that (i) the transport equations derived elsewhere for a single elastic structure hold in each subsystem, and (ii) the power flows at the interface between the substructures are reflected and/or transmitted according to the laws obtained by a wave approach. An analytical derivation of high-frequency power flow reflection/transmission coefficients for the junction of two thick beams or plates has been outlined. It is based on a wave component analysis coherent with the high-frequency transport properties of such structures, and accounts for possible mode conversions at the junction. It also yields the reflection coefficients for a single semi-infinite beam or plate with Dirichlet or Neumann boundary conditions at its end. Numerical examples have been presented where the transport equations are solved by a finite element method or a direct Monte-Carlo method. The emergence of a diffusive regime due to the presence of interfaces and/or boundaries has been demonstrated numerically for an assembly of thick plates impacted by a shear load.

The proposed analytical model is readily useable in the discontinuous Galerkin finite element scheme with weakly enforced generalized interface conditions derived in Savin (2007). What is lacking at present is a transport model for the high-frequency guided waves possibly trapped by non-convex interfaces. The issue of characterizing surface waves in the high-frequency regime is of considerable interest for the many applications in electronics, solid-state physics, acoustics, or geophysics for example. From experimental measurements and practice it is recognized that a significant amount of vibrational energy is likely to be transported along the junctions and interfaces in a complex structure. This fundamental problem is the subject of ongoing research.

References

Akian, J.-L (2003), "Wigner measures for high-frequency energy propagation in visco-elastic media", Technical

Report RT 2/ 07950 DDSS, ONERA, Châtillon.
Akian, J. -L. (2006), "Semi-classical measures for steady-state three-dimensional viscoelasticity in an open bounded set with Dirichlet boundary conditions", Technical Report RT 1/11234 DDSS, Châtillon.
Bal, G., Keller, J.B., Papanicolaou, G., and Ryzhik, L. (1999), "Transport theory for acoustic waves with reflection and transmission at interfaces", *Wave Motion*, **30**(4), 303-327.
Bougacha, S., Akian, J.-L. and Alexandre R. (2007), "Mesure de Wigner dans un domaine borné convexe", In Istas, J., editor, *Actes du Congrès National de Mathématiques Appliquées et Industrielles, Praz-sur-Arly, 4-8 juin 2007*, Paris. SMAI.
Bouthier, O.M. and Bernhard, R.J. (1992), "Models of space-averaged energetics of plates", *AIAA Journal*, **30**(3), 616-623.
Burq, N. and Lebeau, G. (2001), "Mesures de défaut de compacité, application au système de Lamé", *Annales Scientifiques de l'École Normale Supérieure,* **34**(6), 817-870.
Gérard, P., Markowich, P.A., Mauser, N.J. and Poupaud, F. (1997), "Homegenization limits and Wigner transforms", *Communications on Pure and Applied Mathematics*, L(4), 323-379.
Gou, M. and Wang, X.-P. (1999), "Transport equations for a general class of evolution equations with random perturbations", *Journal of Mathematical Physics*, **40**(10), 4828-4858.
Jin, S. and Liao, X. (2006), "A Hamiltonian-preserving scheme for high frequency elastic waves in heterogeneous media", *Journal of Hyperbolic Differential Equations*, **3**(4), 741-777.
Langley, R. S. (1995), "On the vibrational conductivity approach to high frequency dynamics for two-dimensional components", *Journal of Sound and Vibration*, **182**(4), 637-657.
Lapeyre, B., Pardoux, E. and Sentis, R. (1998), "Méthodes de Monte-Carlo pour les Équations de Transport et de Diffusion", **29** *Mathématiques & Applications*, Springer, Berlin.
Lase, Y., Ichchou, M.N., and Jézèquel, L. (1996), "Energy flow analysis of bars and beams: theoretical formulations", *Journal of Sound and Vibration*, **192**(1), 281-305.
Lions, P.-L and Paul, T. (1993), "Sur les mesures de Wigner", *Revista Matemática Iberoamericana*, 9(3), 553-618.
Lyon, R.H. and DeJong, R.G. (1995), *Theory and Application of Statistical Energy Analysis*, Butterworth-Heinemann, Boston, 2nd edition.
Miller, L. (2000), " Refraction of high-frequency waves density by sharp interfaces and semiclassical measures at the boundary", *Journal de Mathématiques Pures et Appliquées*, **79**(3), 227-269.
Naghdi, P.M. and Cooper, R.M. (1956), "Propagation of elastic waves in cylindrical shells, including the effects of transverse shear and rotatory inertia", *Journal of the Acoustical Society of America*, **28**(1), 56-63.
Nefske, D.J. and Sung S.H. (1989), "Power flow finite element analysis of dynamic systems: basic theory and application to beams", *ASME Journal of Vibration, Acoustics, Stress and Reliability in Design*, **111**(1), 94-100.
Norris A. N. (1998), "Reflection and transmission of structural waves at an interface between doubly curved shells", *Acta Acustica/Acustica*, **84**(6), 1066-1076.
Ouisse, M. and Guyader, J.-L. (2003), "Vibration sensitive behaviour of a connecting angle, case of coupled beams and plates", *Journal of Sound and Vibration*, 267(4), 809-850.
Papanicolaou, G.C. and Ryzhik, L.V. (1999), Waves and transport. In Caffarelli, L. and E, W., editors, *Hyperbolic Equations and Frequency Interactions*, pages 305-382, Providence. AMS.
Savin, E. (2004), "Transient transport equations for high-frequency power flow in heterogeneous cylindrical shells", *Waves in Random Media*, **14**(3), 303-325.
Savin E. (2005a), "High-frequency vibrational power flows in randomly heterogeneous structures", In Augusti, G., Schuëller, G.I. and Ciampoli, M., editors, *Proceedings of the 9th International Conference on Structural Safety and Reliability ICOSSAR 2005, Rome, 19-23 june 2005*, pages 2467-2474, Rotterdam. Mill-press Science Publishers.
Savin E. (2005b), "Radiative transfer theory for high-frequency power flow in fluidsaturated, poro-visco-elastic media", *Journal of the Acoustical Society of America*, **117**(3), 1020-1031.
Savin, E. (2006), "Derivation of diffusion equations for high-frequency vibrations of randomly heterogeneous structures", In Topping, B.H.V., Montero, G. and Montenegro, R., editors, *Proceedings of the 8th International Conference on Computational Structures Technology CST 2006, Las Palmas de Gran Canaria, 12-15 September 2006*, Stirlingshire. Civil-Comp Press.
Savin, E. (2007), "Discontinuous finite element solution of radiative transfer equations for high-frequency power flows in slender structures", Preprint 2007.